

Analysis of Curvature Effects on Boundary Layer Separation and Turbulence  
Model Accuracy for Circulation Control Applications

A Senior Project

Presented to:

the Faculty of the Aerospace Engineering Department  
California Polytechnic State University, San Luis Obispo

In Partial Fulfillment  
of the Requirements for the Degree  
Bachelor of Science

by

Daniel Wilde

June, 2010

© 2010 Daniel Wilde

This set of analyses involves flow separation in high curvature regions with special attention to circulation control implementations. Blown flaps of various shapes designed by Rory Golden for use on the AMELIA, or Advanced Model for Extreme Lift and Improved Aeroacoustics, short takeoff vehicle have exhibited flow separation at locations where flap curvature changes. Investigating this problem, its causes, and potential solutions, I have concluded that the separation is equally a function of the flow simulation turbulence model used, and the geometry of the flap itself. Using Gambit version 11.0.1 for grid generation and Fluent version 6.3.26 for CFD calculations, I have investigated both factors, comparing turbulence models to the experimental data of Monson<sup>2</sup> to observe their accuracy in high curvature regions, and designed a set of flap geometries which I subjected to high circulation conditions that exhibit the Coanda effect to compare separation tendencies.

## Nomenclature

$C_{\mu}$	Blowing coefficient, $= \frac{\dot{m}_{slot} U_{slot}}{q_{\infty} S}$
M	Mach number
P	Stagnation pressure
S	Reference area for nondimensionalizing force coefficients
p	Static pressure
$\gamma$	Ratio of specific heats = 1.4 for air

### *subscripts*

slot	Conditions at jet slot
$\infty$	Conditions at freestream

### *conventions*

AMELIA	Advanced Model for Extreme Lift and Improved Aeroacoustics
CFD	Computational Fluid Dynamics

## I. Introduction

The AMELIA is a circulation control vehicle designed used, in part, to develop circulation control modeling techniques<sup>10</sup>. Some of the work performed on the design is sponsored by the Department of the Navy, Office of Naval Research, under award #N00014-06-1-1111, with the majority funded as part of a NASA Research Announcement award under Contract #NNL07AA55C with Craig Hange and Clif Horne as the technical monitors.

The circulation CC high lift system of AMELIA incorporates upper surface blowing on trailing edge flaps. The Coanda effect, or the tendency of high speed flow to follow a curved surface<sup>11</sup>, causes the high speed flow to change direction, following the flap surface as it curves downward. This flow also entrains much of the freestream air above the wing, deflecting it downward. Ultimately, by forcing circulation and deflecting air downward, the system generates high lift.

Previous work on the flap geometry and circulation control of the AMELIA exhibited flow separation on the dual radius flaps used at the point of radius change, which this report investigates<sup>9</sup>. The first factor that must be addressed when investigating predicted flow separation is the accuracy of the model used. Golden performed initial flap design using a standard k-epsilon turbulence model within the Fluent software. Based on research by Moser<sup>5</sup>, Rumsey<sup>1</sup>, Bardina<sup>7</sup>, and Bell<sup>6</sup>, however, k-  $\epsilon$  turbulence models poorly model circulation control scenarios. Two assumptions made in this model are that streamline curvature is negligible, and that eddy viscosity behaves linearly. Neither of these assumptions holds true in the case of blown flaps. Jet flow eddy viscosity behaves non-linearly, and the flap surface is highly curved relative to boundary layer thickness. Moser has suggested that a Reynolds stress formulation includes terms neglected by the k-epsilon model and performs valid analysis.<sup>5</sup>

Because the separation under investigation appears to be a function primarily of curvature, my research has focused primarily on curvature effects in wall bounded flows, without strong focus on eddy viscosity. Research into the mechanisms of flow behavior on curved surfaces is poorly understood, but many attempts have been made to improve this understanding. Much of this work attributes rotation effects to Taylor-Gortler vortices<sup>5</sup> and viscous

instabilities. Much of the work suggests that in order to accurately model circulation control or highly curved flow, a full Reynolds-stress analysis, which is computationally expensive and unstable, should be used.

Turbulence models have been formulated which do not make the assumptions involved in the standard k-epsilon model. These models include, RSM, SARC<sup>3</sup>, k-epsilon v<sup>2</sup> f, and EASMCC. The RSM model is a Reynolds stress formulation as recommended by Moser<sup>5</sup>. The SARC model is a standard 1 equation Spalart Allmaras model with a streamline curvature correction term. This term essentially rotates the principal strain axes of the flow as the flow direction rotates. The SARC model outperforms the original SA formulation in situations of high curvature, but poorly represents other flow characteristics.<sup>4</sup> The v<sup>2</sup> f model has been researched and implemented in Fluent by Travis Storm<sup>8</sup>, also working on the AMELIA project. He has found that overall lift and drag predictions using his turbulence model on the CC wing of the AMELIA match overall lift and drag numbers, but poorly represent local flow characteristics. The EASMCC or explicit algebraic stress model (curvature corrected) has been shown by Rumsey<sup>1</sup> to calculate flow variables on curved surfaces of high curvature with reasonable accuracy.

The turbulence models compared in this analysis include standard Spalart Allmaras, standard k-epsilon, realizable k-epsilon, shear stress transport k-omega, RSM, and the k-epsilon v<sup>2</sup> f model developed by Travis Storm. Using experimental data collected by Monson<sup>2</sup>, for a U-shaped duct I have compared the accuracy of each of these models in a high curvature scenario.

In addition to comparing turbulence models, this report also documents a comparison of blown flap shapes in an implementation similar to that of the AMELIA. Comparing several flaps of dual radius, linearly increasing radius, and quadratically increasing radius to a constant radius flap I observe the effect of curvature variation on circulation control flow separation.

The combination of these simulations is intended to enhance the understanding of separation and its modeling in high curvature flow, and provide a basis for improving future circulation control flap designs.

## II. U-duct Study

Experimental data for flow through a U-duct geometry shown in Figure 1 has been studied by Monson<sup>2</sup> and other fluid dynamicists including Bell<sup>6</sup> to compare the ability of turbulence models to capture the effects of wall curvature.

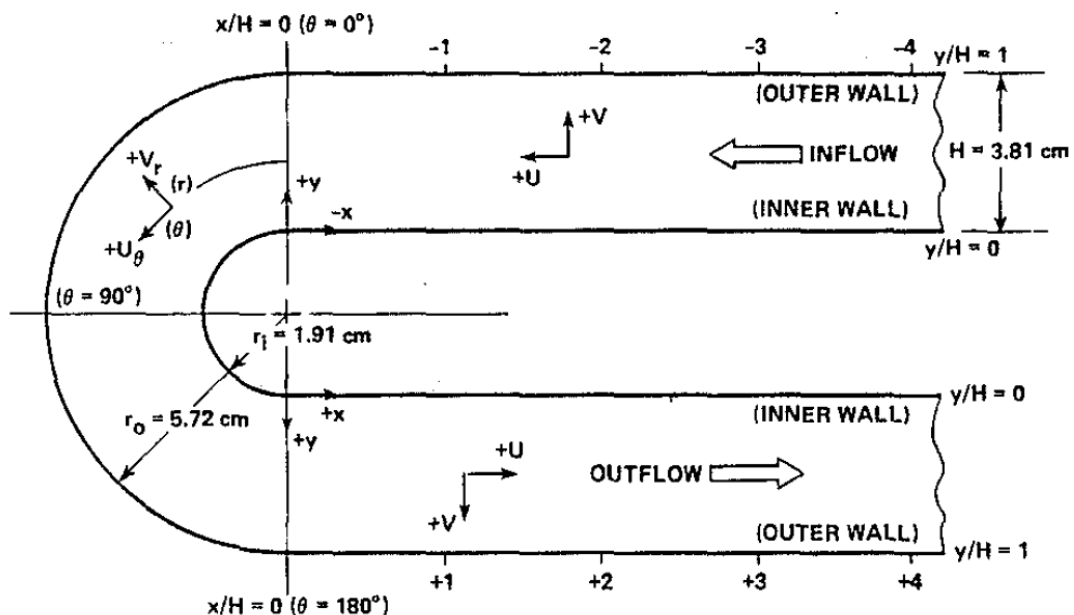
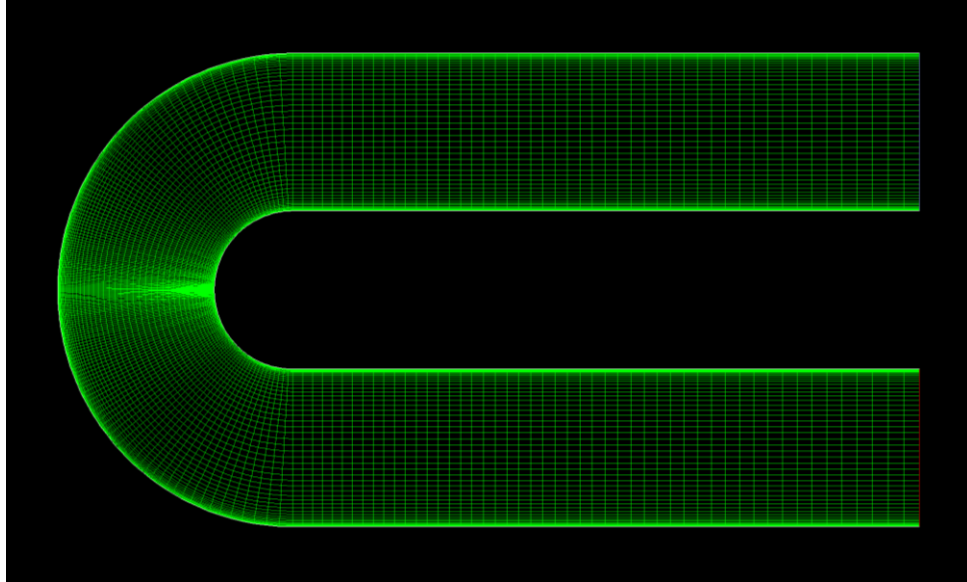


Figure 1. U duct geometry with dimensions<sup>2</sup>

A mesh was built of this geometry using Gambit with a  $y^+$  value less than 1 for flow at 32 m/s and 1.2 atm, corresponding to the experimental data at a Reynolds number of  $10^5$  and is shown in Figure 2. U grid mesh



**Figure 2. U grid mesh**

The mesh was loaded into Fluent where different turbulence models could be applied. To achieve the desired flow speed of 32 m/s, a pressure inlet at the duct inflow was set to 730 Pa below the operating pressure of 1.2 atm to accommodate the prescribed total pressure of 1.2 atm minus dynamic pressure based on Isentropic pressure equation, eqn. 1. Then, a pressure outlet was defined at the duct outflow and its pressure decreased until the velocity at the duct inlet converged to 32 m/s.

$$\frac{p}{p_0} = \left(1 + \frac{\gamma-1}{2} M^2\right)^{\frac{-\gamma}{\gamma-1}} \quad (1)$$

Velocity profiles at  $0^\circ$ ,  $90^\circ$  and  $180^\circ$  as labeled in Figure 1 and velocity contours included in appendix 1 are used to compare the models throughout the curvature of the duct. Figure 3, Figure 4, and Figure 5 include the velocity profiles for the built in Fluent turbulence models analyzed as well as experimental data and a first order linear solution of the Storm<sup>8</sup>  $v^2 f$  model.

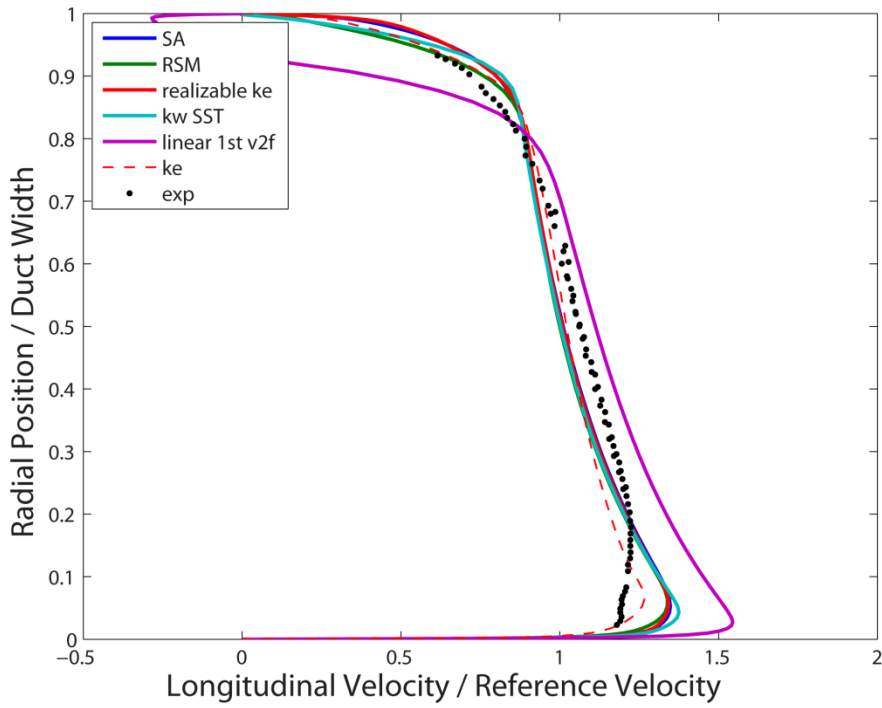


**Figure 3. U-Duct velocity profiles at 0 degrees of rotation**

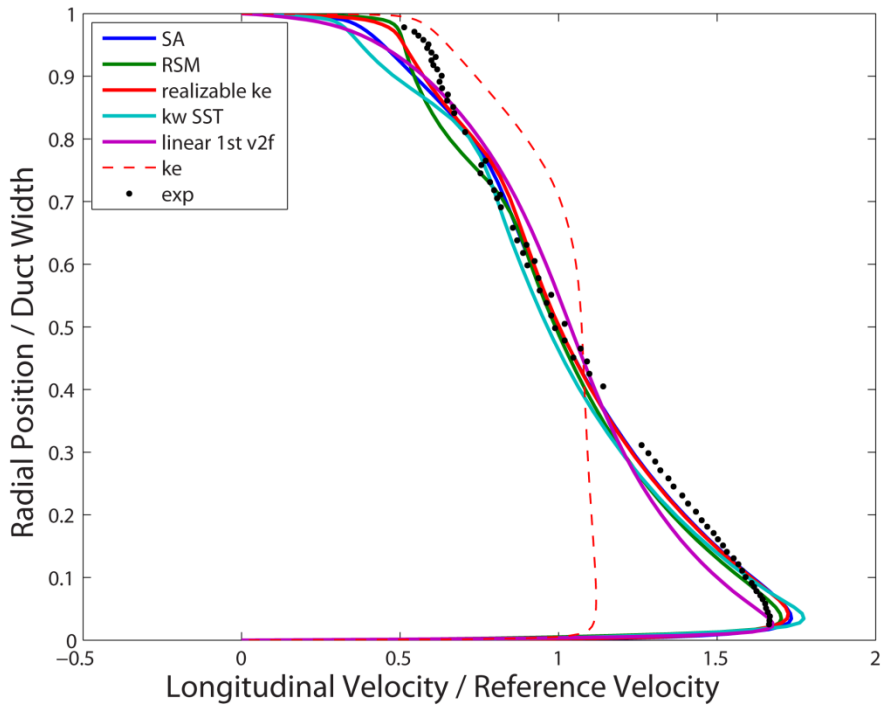


**Figure 4. U-Duct velocity profiles at 0 degrees of rotation**

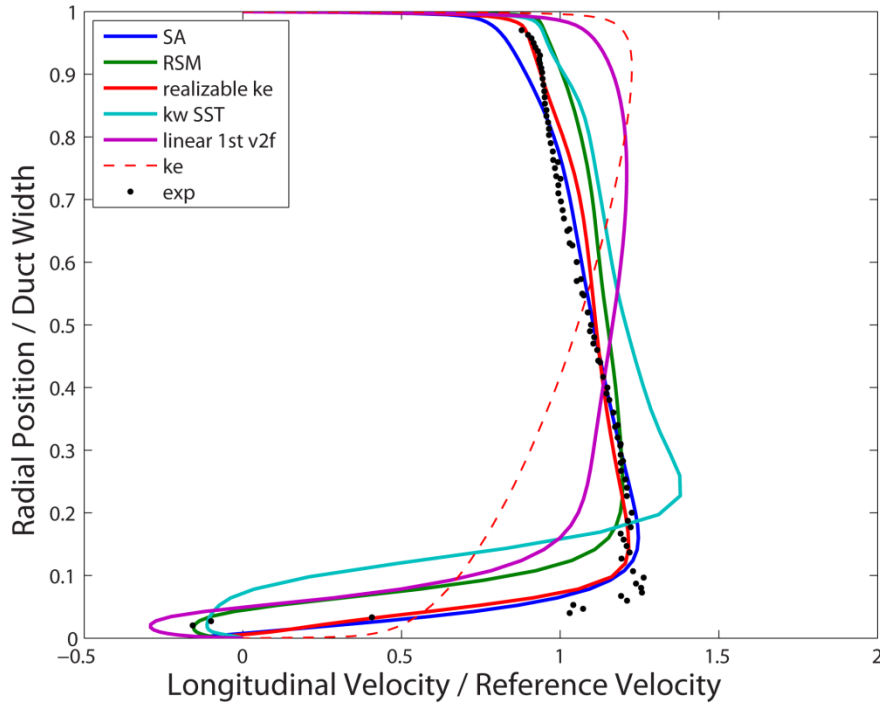


**Figure 5. U-Duct velocity profiles at 0 degrees of rotation**

Aside from the standard k- $\epsilon$  model which poorly represents this flow, the discrepancies between various models and experiment occur near the walls of the duct. These differences include variations in boundary layer thickness and presence of recirculation. Table 1 compares the accuracy of the models near the wall on a scale of 1 to 10, as well as their computational stability, which determines the amount of time and resources required to run the model.

**Table 1. Summarized performance of various turbulence models**

	Boundary layer thickness	recirculation	Computational Stability
SA	8	1	7
RSM	7	9	1
Realizable k- $\epsilon$	8	1	8
SST k- $\omega$	6	7	9
Standard k- $\epsilon$	1	1	10

A benefit of this study is that it can be used to compare the accuracy of new or unfamiliar models. In addition to the first order linear  $v^2 f$  solution from Figure 3, Figure 4, and Figure 5 second order linear, first and second order nonlinear, and first and second order nonlinear with curvature correction solutions for the Storm k- $\epsilon$   $v^2 f$  model were obtained. The resultant velocity profiles of the linear and nonlinear models are compared independent of the built in Fluent models in Figure 6 Figure 7 Figure 8.

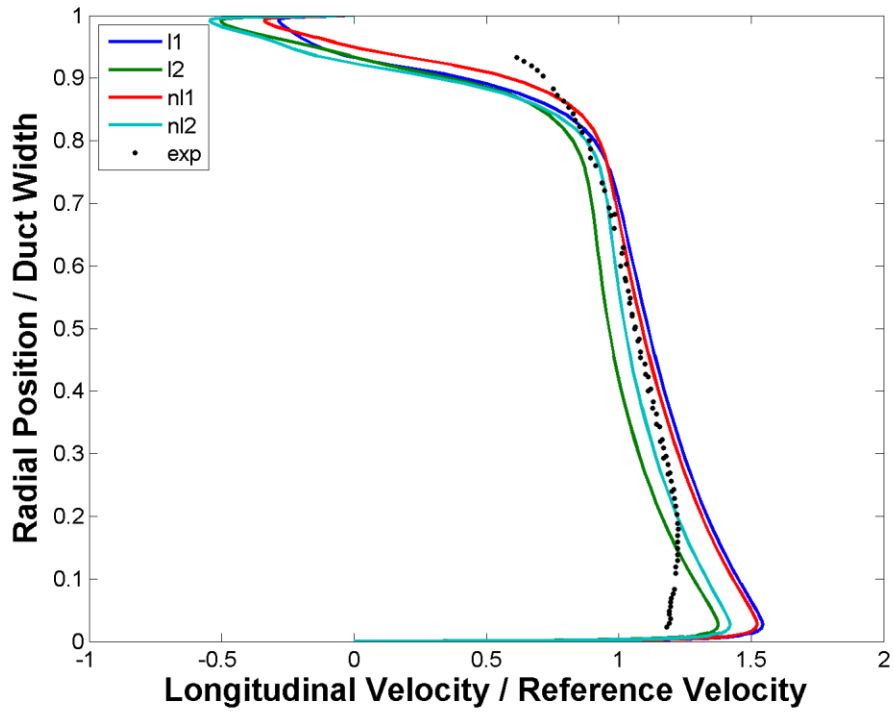


Figure 6. Velocity profiles at 0 degrees of rotation for  $v^2 f$  models

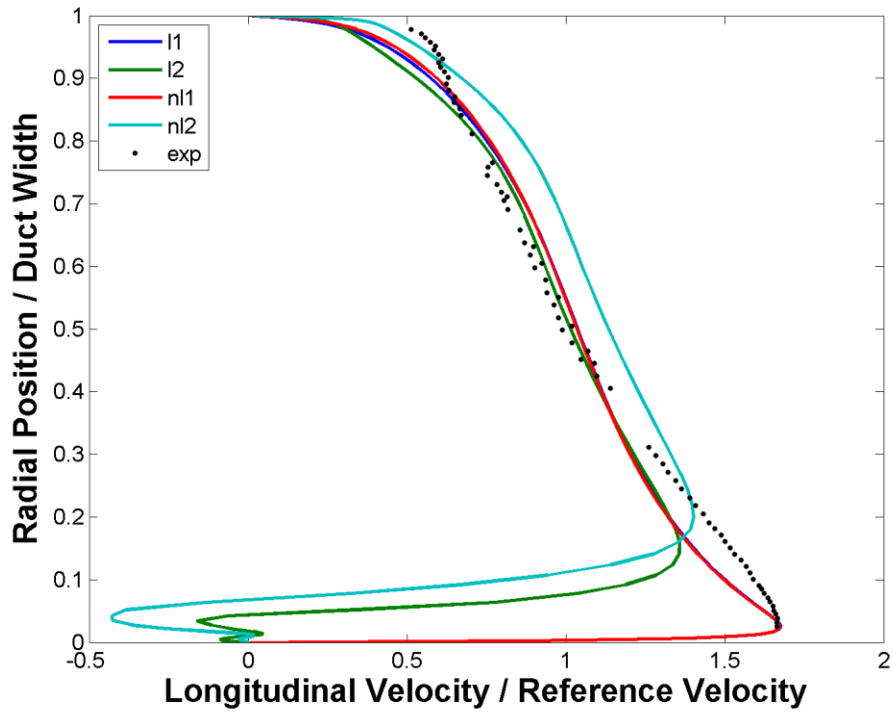
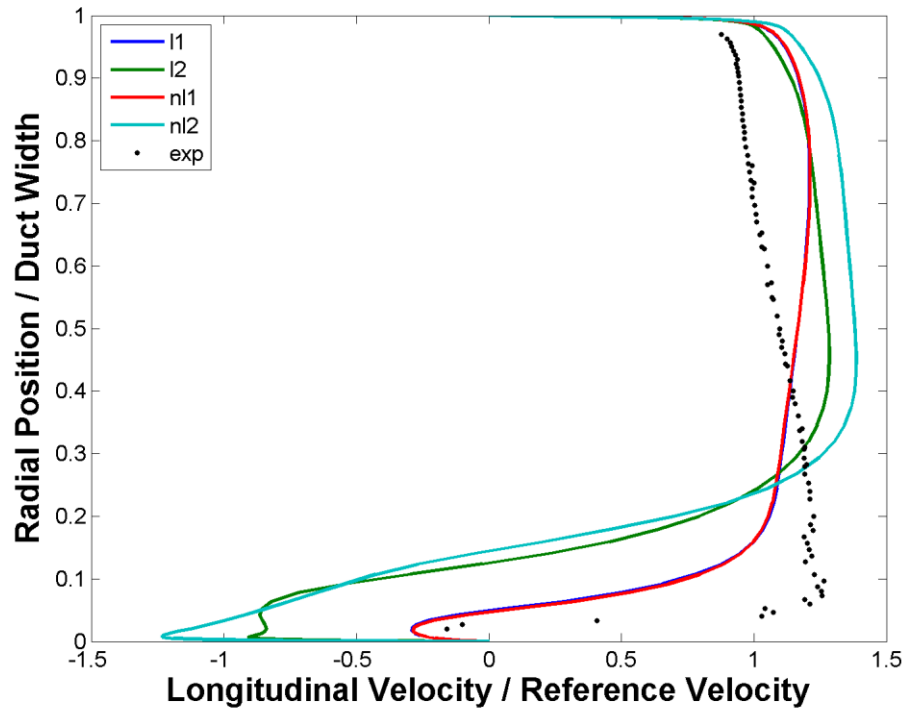


Figure 7. Velocity profiles at 90 degrees of rotation for  $v^2 f$  models



4

**Figure 8. Velocity profiles at 0 degrees of rotation for  $v^2 f$  models**

The behavior of the  $v^2 f$  models in high curvature can be analyzed based on this simulation. Both linear and nonlinear models perform reasonably well when run first order, closely matching the experimental separation and recirculation at the inner wall at 180 degrees of rotation. However, they do over predict the amount of separation on the outer wall at 0 degrees. It is also interesting that these first order simulations behave somewhat like the standard  $k-\epsilon$  model at 180 degrees of curvature, in that the maximum predicted velocity occurs near the outer wall and decreases near the inner wall. All of the other models, along with experiment, have predicted the opposite.

Next are the second order solutions. It appears that the second order  $v^2 f$  models over predict recirculation induced in the U duct. We can see that inner wall recirculation is predicted starting at 90 degrees, and by 180 degrees, recirculation is expected at a full 32 m/s opposite the primary flow in the duct.

By capturing flow physics near the wall, the 1<sup>st</sup> order  $v^2 f$  solutions provide a clear improvement compared to the standard  $k-\epsilon$  model, but it seems that the sensitivity to circulation may be exaggerated in the second order simulations. The differences between the linear and nonlinear solutions are much less pronounced than that between the 1<sup>st</sup> and 2<sup>nd</sup> order.

Due to an error with the renewal of the department's Fluent licenses, I was not able to make velocity plots of the nonlinear curvature corrected solutions for this flow, but have included velocity contours for all 6  $v^2 f$  cases in Figure 9.

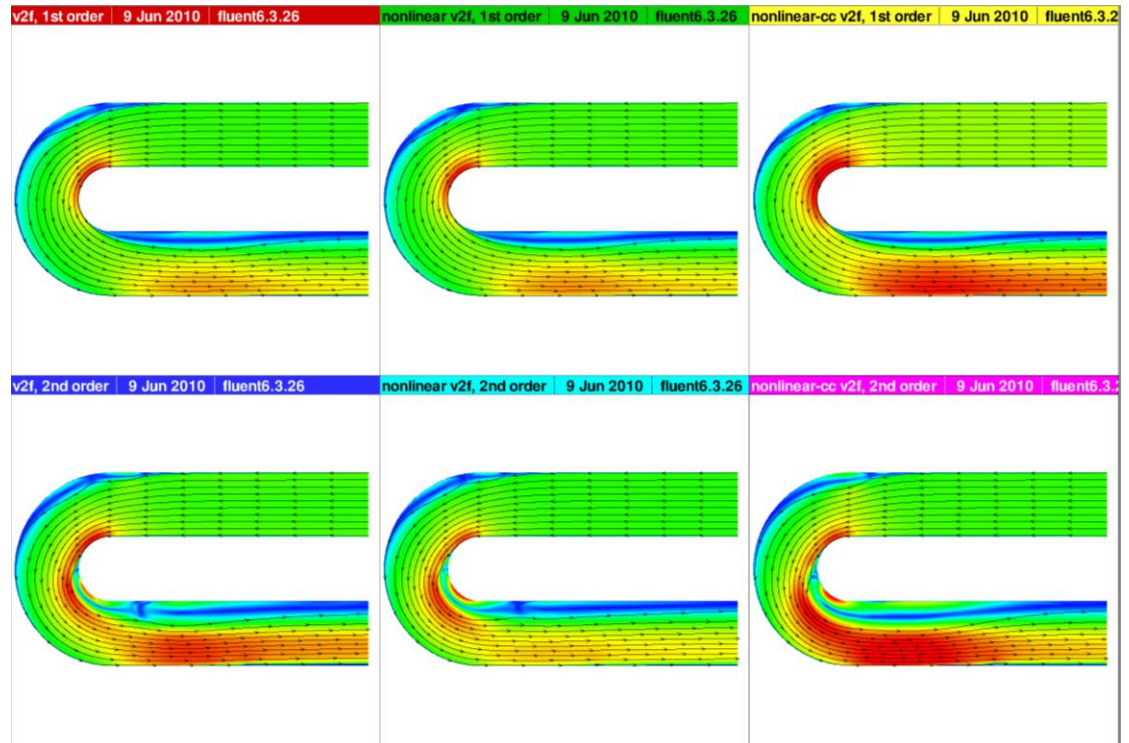


**Figure 9. Velocity contours of U-duct using  $v^2 f$  models**

Based on these contours, it appears that the differences between the 1<sup>st</sup> order curvature corrected models does not affect separation or recirculation predictions strongly, but increases the amount of inner wall acceleration within the curve and results in more high speed flow near the outer wall downstream of the bend. The second order curvature corrected model differs from the other 2<sup>nd</sup> order models as well. It appears that the same degree of separation occurs, but with a larger recirculation region. In addition, we again see an increase in the velocity gradient within the duct downstream of the bend. However, it appears that, unlike the rest of the  $v^2 f$  solutions, the second order cc model predicts a lower velocity at the outer wall than near the inner wall separation region. This suggests that the curvature correction corrects some of the standard  $k-\epsilon$  model behavior which makes it not suitable for high curvature regions. Further information on these models can be obtained in Storm's paper<sup>8</sup>.

Performing the U duct study allowed me to assess the performance of many turbulence models in a high curvature region representative to the geometry of a circulation control flap. Though the RSM model most accurately predicts the flow in the U-Duct, the SST  $k-\omega$  model was chosen for use on my flap shape study for its ability to capture recirculation, combined with its fast and stable iterations.

### III. Blown Flap Geometry Study

Flow separation involves complex physical phenomena, but essentially occurs when flow energy becomes too low to maintain attachment. In the case of AMELIA's blown flaps, the wall flow from the jet is very high energy and, as the flow moves along the flap, becomes less energetic. This is the reasoning behind the dual-radius geometry with a greater radius further downstream in the flow where energy is decreased. However, geometry with continuous curvature should, intuitively, improve flow attachment by more consistently varying with the energy of the flow. Golden's research has shown that, a continuous change in curvature is less prone to separation due to the elimination of a discontinuity of surface curvature<sup>9</sup>.

As a means of studying the effects of flap curvature on flow separation I created a baseline flap with a constant radius of 1m to compare other geometries to, shown in Figure 10.

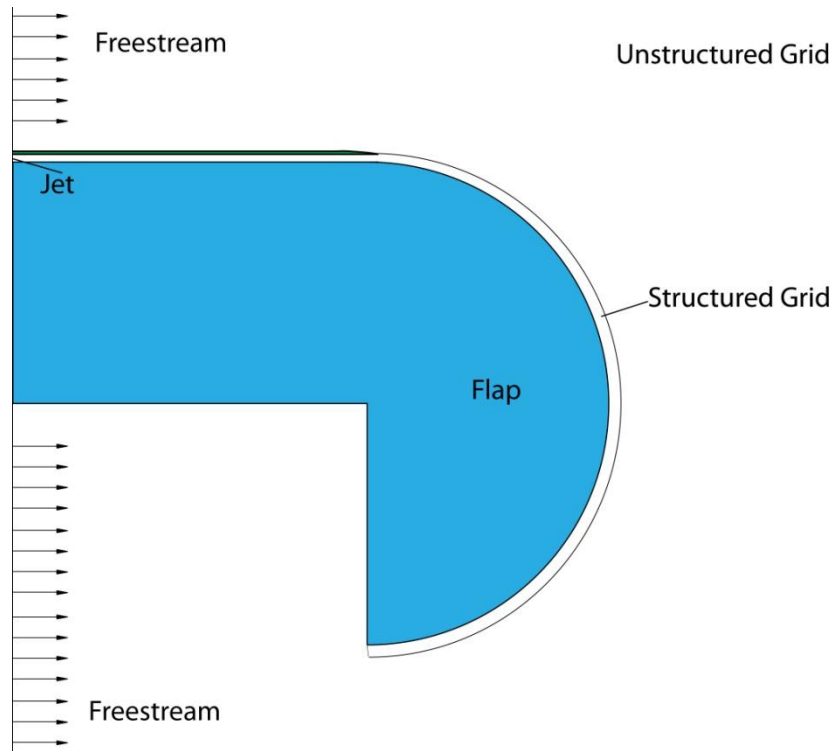


**Figure 10. constant radius flap geometry with mesh**

I then created a series of flap geometries to compare their separation tendencies based on 2 variables; ratio of radius increase, and radius change type. Ratio of radius increase refers to the ratio of the flap after 180 degrees of turning to the initial radius of curvature of the flap where the jet flow is released while radius change type refers to the way the radius increases, including dual radius, linearly increasing radius, and quadratically increasing radius geometries. All geometries were created such that their average radius matched that of the baseline constant radius flap. The series of linearly varying radius flaps is illustrated in Figure 11, Figure 12, and Figure 13.

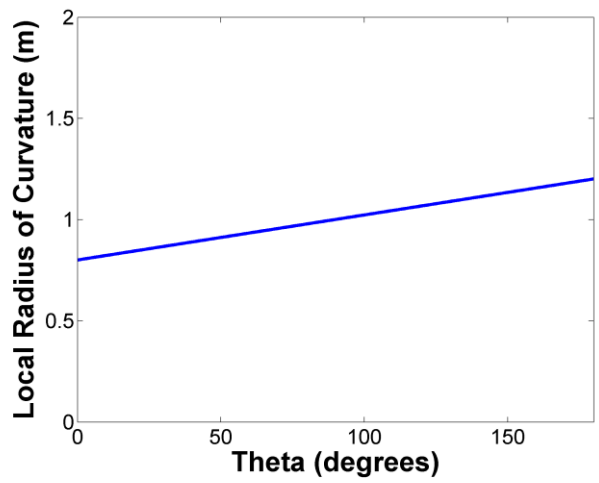
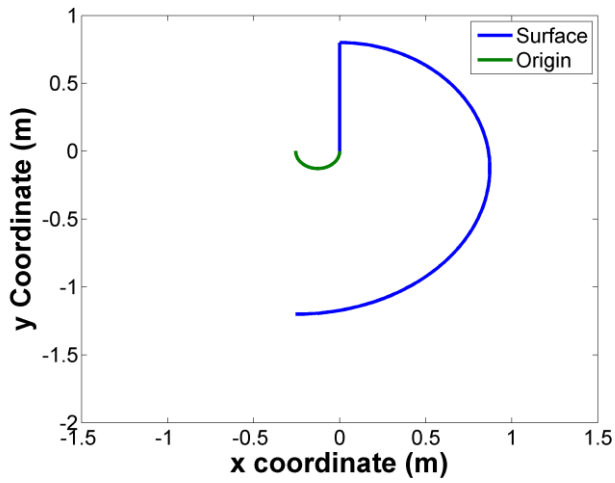


Figure 11. Linear radius change flap with 1 to 1.5 radius ratio

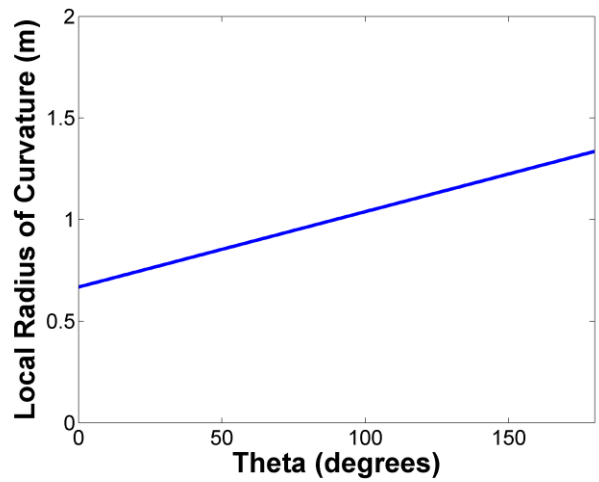
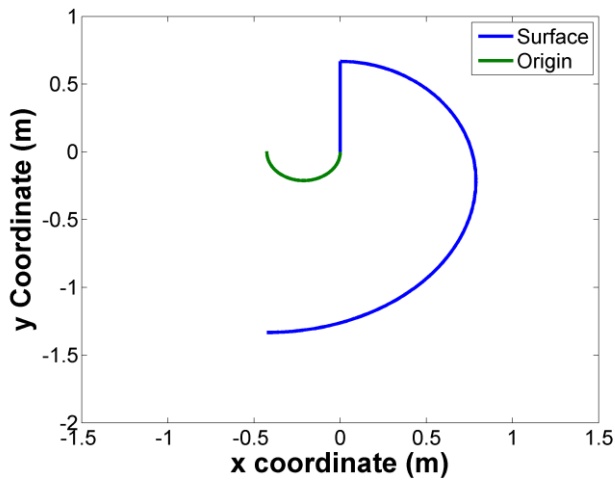


Figure 12. Linear radius change flap with 1 to 2 radius ratio

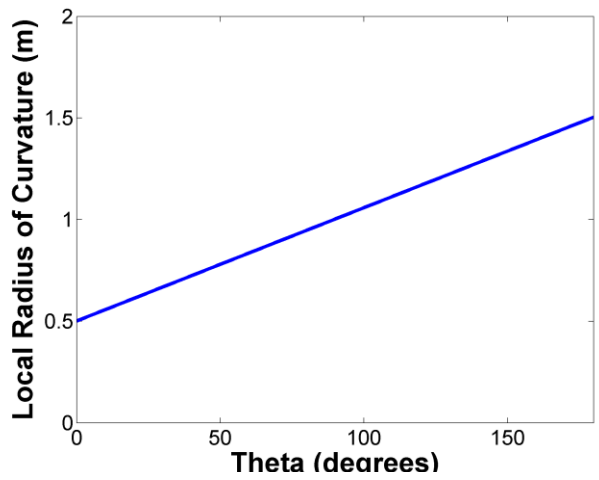
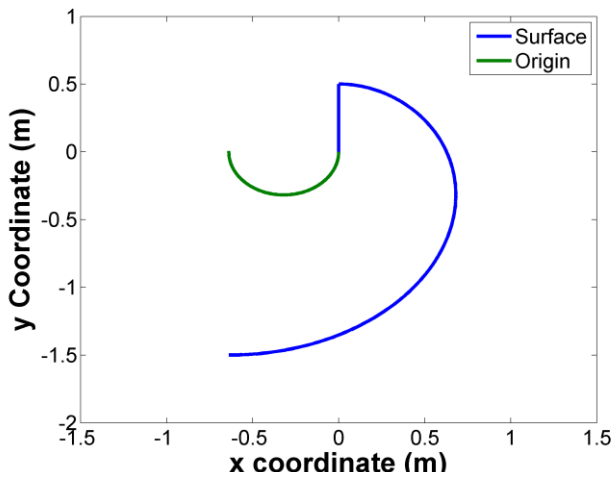


Figure 13. Linear radius change flap with 1 to 3 radius ratio

Shown are the flap shape, locations of the geometric origin, and actual radius of curvature throughout the rotation of the flap. The same information is presented for the series of quadratically varying radius flaps in Figure 14, Figure 15, and Figure 16.

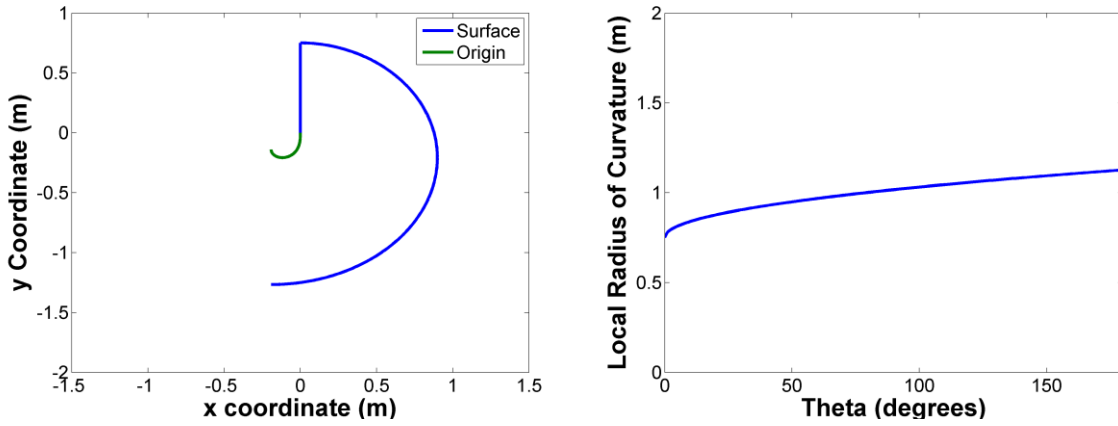


Figure 14. Quadratic radius change flap with 1 to 1.5 radius ratio

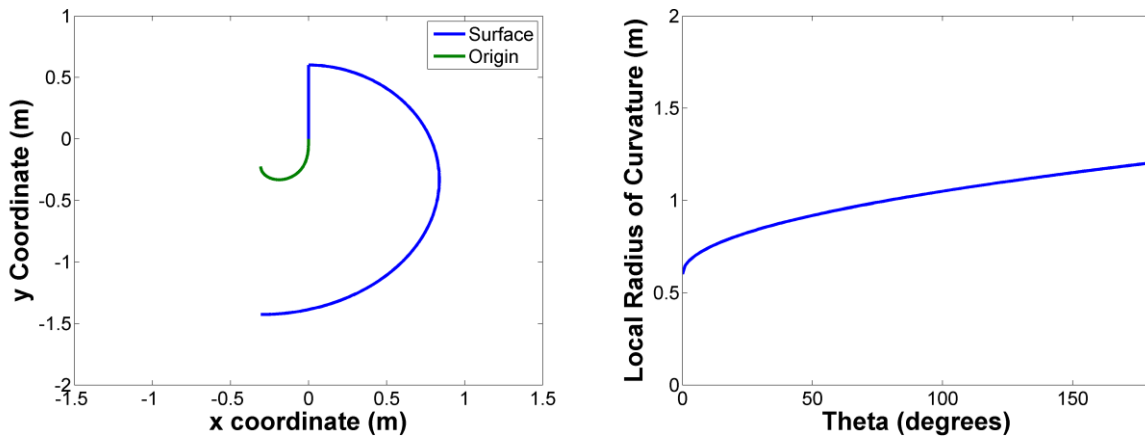


Figure 15. Quadratic radius change flap with 1 to 2 radius ratio

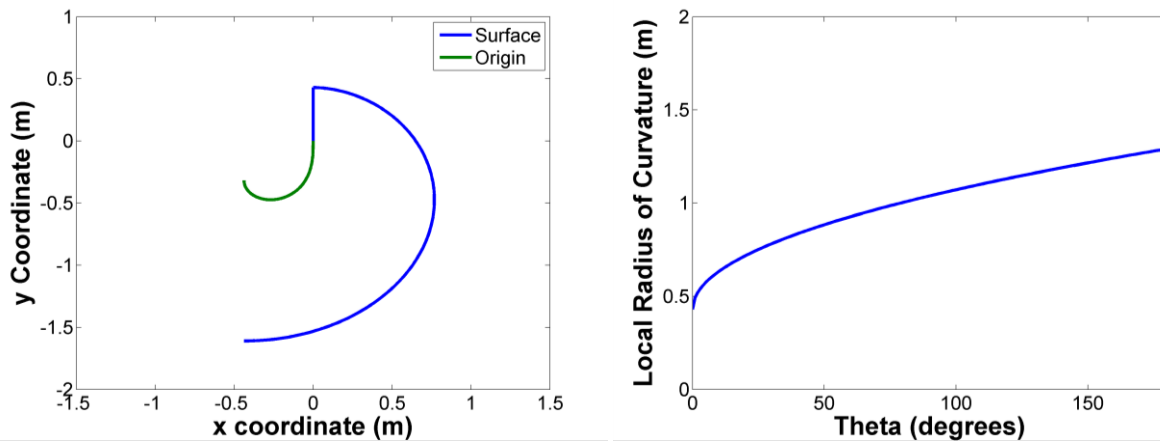
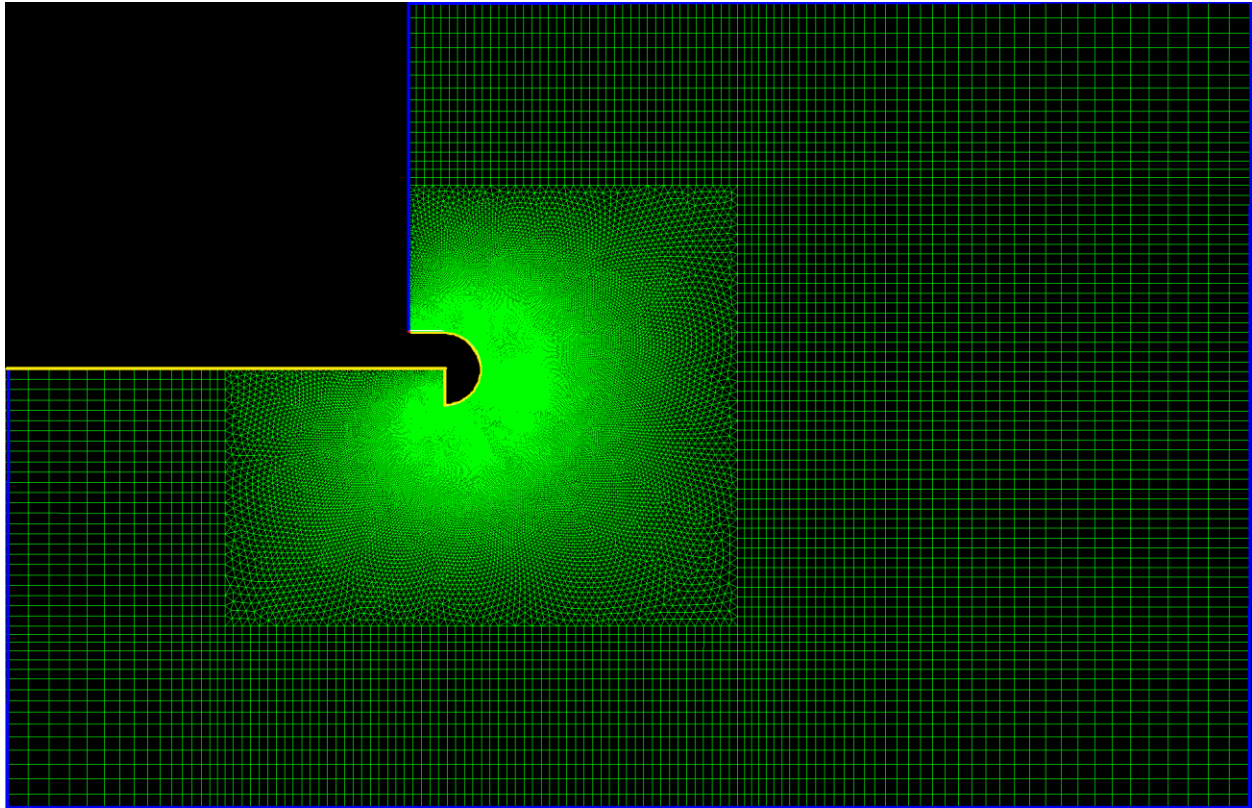


Figure 16. Quadratic radius change flap with 1 to 3 radius ratio

A series of dual radius flaps was also created using Gambit that had an initial radius for the first 90° of rotation and a second radius of 1.5, 2, and 3 times the initial radius for the second 90° of rotation. From now on, flaps may be referred to by their shape type then radius ratio, such as linear 2 or dual radius 1.5. I chose dual radius, linearly, and quadratically varying radius flaps to observe the separation on surfaces exhibiting discontinuous radius variation, first order variation and second order variation. This allows me to observe if the smoothness of radius change or rate of radius change improves attachment. For each of these 9 flap shapes as well as the constant ratio baseline flap, a mesh was constructed. The mesh for the constant radius flap is shown in with the far field pressure boundary in blue, walls in yellow, and the jet pressure boundary in red.



**Figure 17. Mesh of constant radius flap**

The  $y^+$  value of this mesh is 1 for jet flows at 340 m/s at standard sea level conditions which the simulations were run at, eliminating the need to use wall functions. The jet itself is shown with mesh in Figure 18.

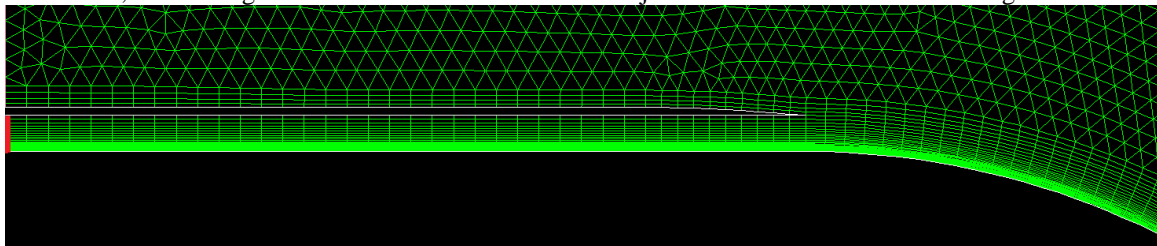


**Figure 18. Jet slot with mesh**

A high pressure inlet indicated in red forces air down the channel between the splitter and flap surface to create jet flow. The splitter then ends as the flap begins to curve. Because the purpose of this study is to observe the interaction between the wall and the flow, special attention was dedicated to the formation of a suitable boundary layer mesh. A structured mesh was created between the flap surface and splitter that extends 180° around the flap surface between the flap surface and an imaginary curve that starts at the end of the splitter. A secondary boundary layer was formed using the boundary layer tool in Gambit on the upper surface of the splitter in the free stream flow

which meets the structured boundary layer grid at the end of the splitter and follows it around the flap along the imaginary curve. The meshes were then loaded into Fluent and the boundary conditions set up according to Table 2.

**Table 2. Operating conditions for flap study**

Operating Conditions	
Operating Pressure	1 atm
Far Field	Mach 0.2 (68 m/s)
Jet inlet	19000 Pa (to achieve 340 m/s)
Momentum Coefficient	0.35
Jet slot height	0.045 m
Average Flap Radius	1 m

The operating pressure and far field velocity are intended to be representative of an aircraft at takeoff or landing when blown flaps would be used while the slot width and  $C_{\mu}$  were based on typical numbers from Coanda effect experimentation<sup>11</sup>. The jet inlet pressure was selected to achieve maximum jet velocity near a Mach number of 1. I also chose to implement a wall boundary upstream of the bottom surface of the flap to mimic the bottom of a wing, representative of the situation the flap would actually be implemented in.

I attempted to use the RSM model on this simulation due to its high accuracy but convergence was slow and sensitive, so I opted to use the faster and more stable  $k-\omega$  model which also captures recirculation as indicated in my U-duct study, but requires less computational time and does not diverge as easily. The converged velocity contours for the constant radius baseline flap are shown in Figure 19.

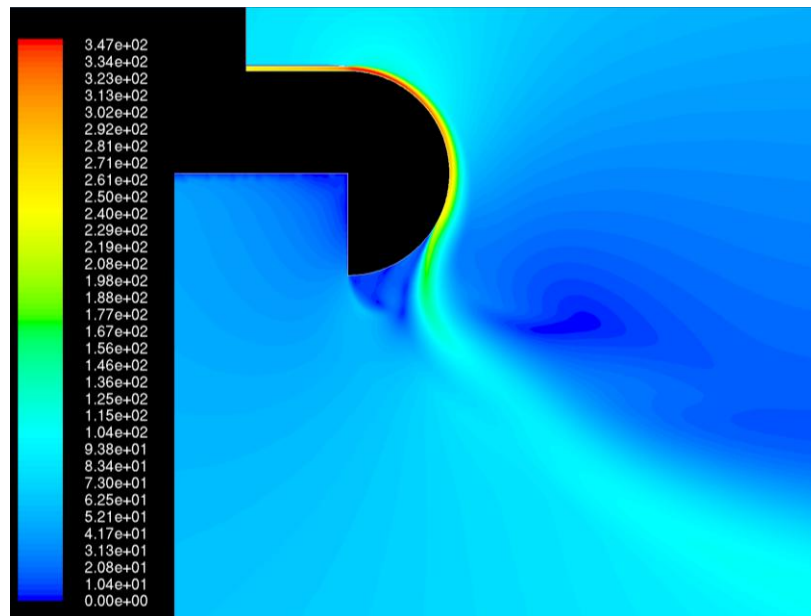


**Figure 19. Velocity contours of constant radius flap**

The high speed jet flow follows the surface of the flap up until the darker blue region on the bottom of the flap which represents low speed, separated flow. We can see in Figure 20 that the domain size allows for the pressure and velocity gradients in the flap region to diffuse.

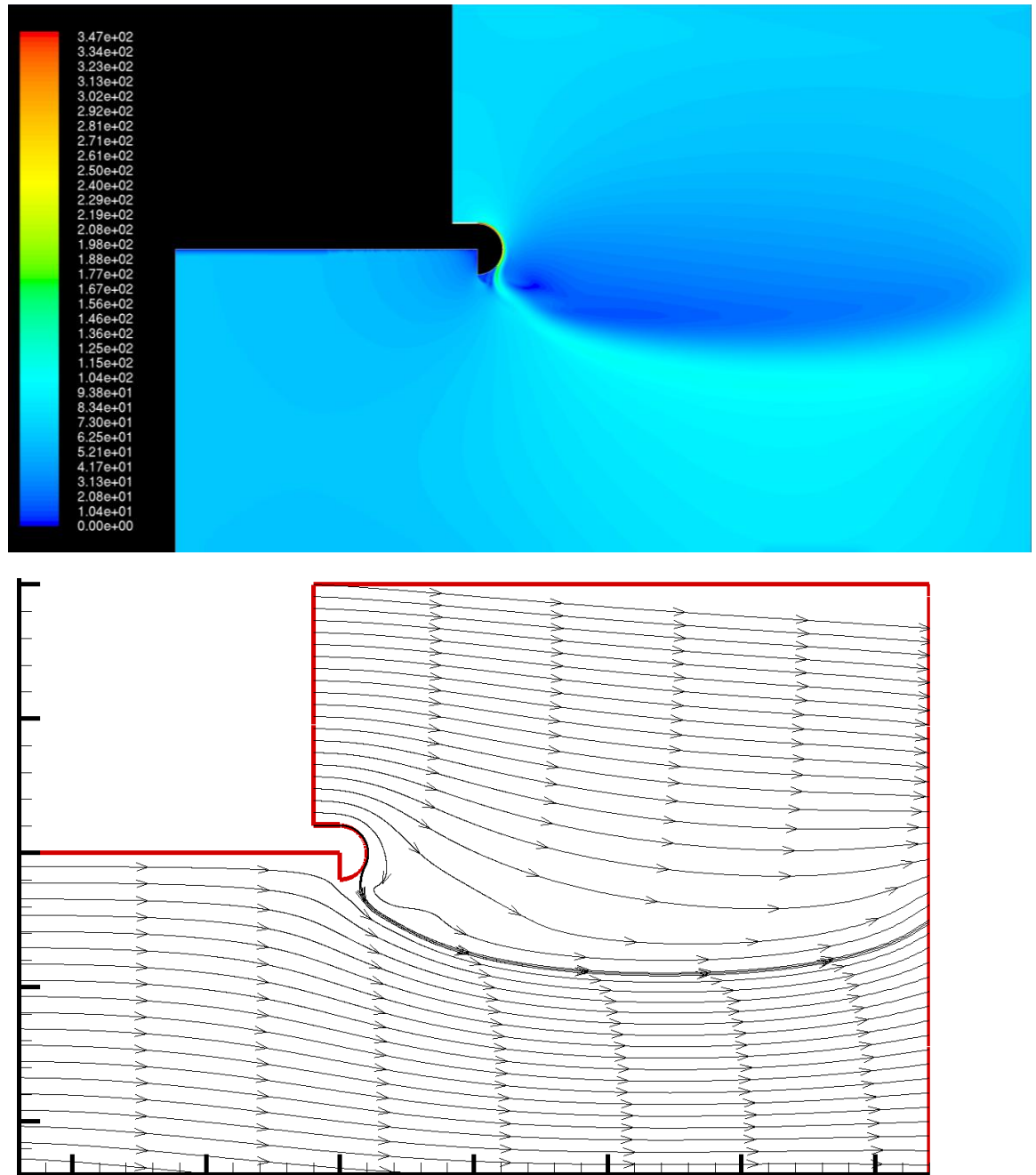


**Figure 20. Computational domain for constant radius flap with velocity contours and with streamlines**

This image also clarifies the domain and boundary conditions that have been explained and illustrates the downward deflection of the freestream air, which creates the lift associated with circulation control systems. Velocity contours performance of the varying radius flaps are displayed in Figure 21 and included more completely and appendix B.

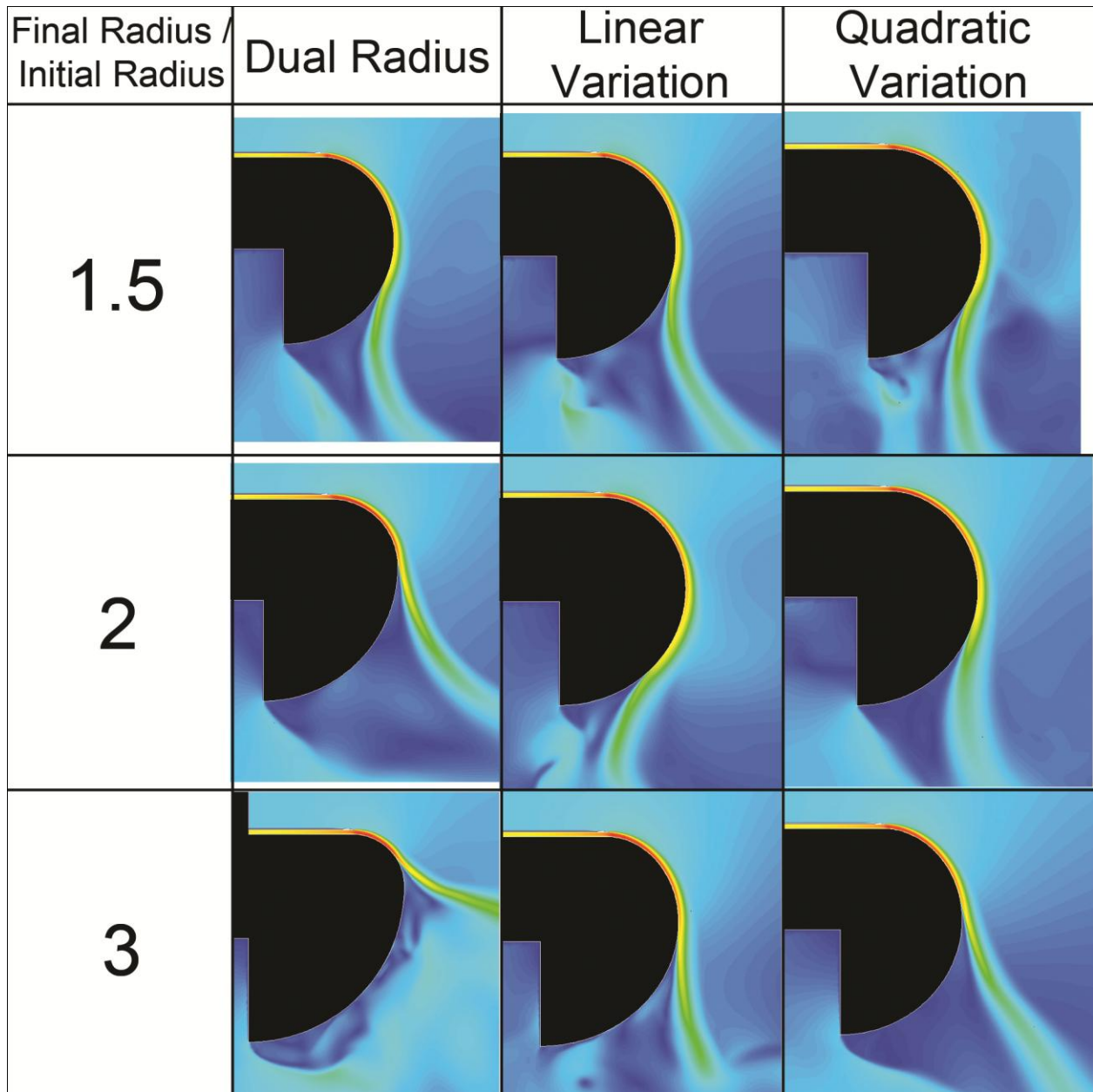


**Figure 21. Performance of blown flap geometries**

Many conclusions can be drawn from the results of this study. Only 2 of my configurations, namely the linear with radius ratio of 2 and quadratic with ratio of 1.5, are able to match the performance of a constant radius flap. This suggests that care should be taken in flap design as increasing radius downstream is not necessarily beneficial. In fact, it appears that change in flap radius destabilizes flow and contributes to separation. At the same time, the linear flap with a radius ratio of 2 clearly outperforms the constant radius flap, meaning that a suitable radius distribution can be beneficial for use on blown flaps.

Another thing to note is that at no radius ratio does the dual radius flap outperform the others, giving credence to the supposition that it is more beneficial to tailor the radius at each point to the flow conditions, than use a discontinuous set of 2 radiuses.

It's also important that no series of flap does the best across the board. This suggests that a straight line or square root function does not define an optimum flap, but rather, each location on the flap has an

optimum radius and that radius must be determined at each angle to design a truly optimum blown flap. This theory is reinforced by the fact that, as shown in, the linear 2 flap and quadratic 1.5 flaps have comparable radii throughout most of their rotation.

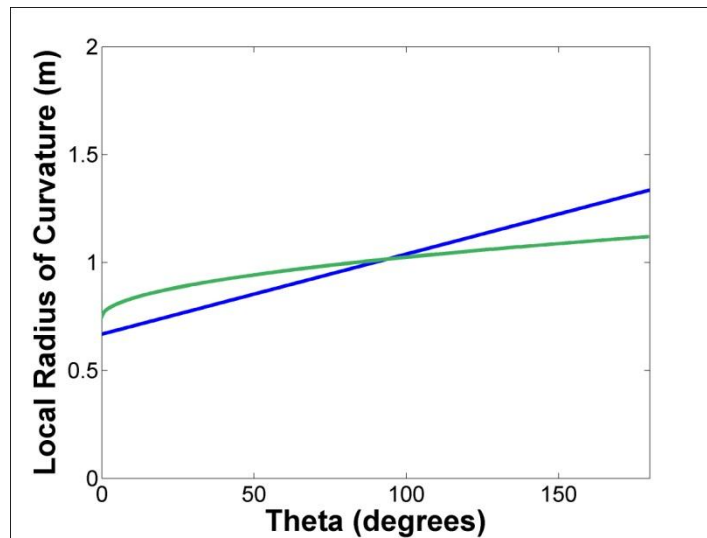


**Figure 22. Comparison of radii of linear radius ratio 2 and quadratic radius ratio 1.5 flaps**

The fact that these flaps also exhibit the best performance suggests that, for the flow I am studying, the optimum radius exists within that region, while flaps like the linear 1.5 that start with a larger radius in the first 90 degrees lose performance along with those with smaller initial radii such as all of the radius ratio 3 flaps. I theorize that a curvature variation can be found that matches the optimal radius of flap curvature at every point and suggest that this variation could be used to generate a flap geometry that maintains flow separation optimally.

One last thing to note is that the set of flaps with a radius ratio of 3 performs worse than those of lower ratios. This suggests that making a significant change in radius is detrimental to flow attachment. Many flaps, however, are designed for both high lift and a cruise condition, in which case the curvature at the trailing edge of the flap should be very small to minimize drag at cruise. This presents a significant problem in that it would be difficult to design a flap that maintains jet flow attachment and cruises efficiently.

I hypothesize that, for a given flow and angle of rotation along a flap, at every point along the flap, there is an optimum radius which allows the flow to remain attached while removing the least energy possible from the flow and allowing for optimum attachment with minimal jet flow energy. In order to verify this hypothesis in the future, I suggest the following options. Ideally, an iterative scheme could be built that would step along the flap and change the radius in small intervals, converge a CFD case, integrate the velocity within the jet flow to see if that reduced or increased the energy of the flow, then change the radius again until an optimum is reached, then repeat that at the next angular position on the flap, iterating from 0 degrees to the end of the flap over and over until an optimum shape is converged upon within a while loop. However, the computational resources required to perform this style of optimization would be staggering.

Instead, I suggest a physical experiment. A deformable sheet of metal could be bent 180 degrees into the form of a basic flap and mounted between 2 sidewalls in such a way that its shape can be changed. Rods attached to the inside of the metal sheet and extend between the sidewalls could be moved within slots in the sidewalls, and tightened into place. A compressor could then be used to blow high speed flow tangential to the top of the experimental flap, and the geometry of the flap could be changed real time until a shape is found that maintains attachment optimally.

In addition to these optimization methods, a simpler validation could be performed by expanding the data set presented in this report. Variations could be made to the linear 2 flap shape and their effect on the flow attachment observed. With enough trial and error, a radius variation will be obtained that enhances flow attachment.

An important consideration to make is that any optimized flap will be optimized for specific conditions. If the ideal curvature is based on flow energy, changing inputs like  $C_{\mu}$  or freestream velocity will create an off-design scenario for which the flap is not optimum.

#### **IV. Conclusion**

By performing the analysis outlined in this report, I have found that many considerations must be made when designing a high lift system that utilizes the Coanda effect, or any highly curved aerodynamic body. Particularly, the simulation model used must be appropriate for the situation. The standard  $k-\epsilon$  model used often in flow simulation has been shown to poorly represent flow behavior in highly curved regions such as those used in circulation control. For this reason, I recommend that simulation and design of blown flaps or similar devices be done using and full RSM model or at least a model that captures recirculation such as the  $k-\omega$  SST model or  $v^2 f$  models.

Also, there is much to be gained or lost in the design of circulation control flaps. Dual radius flaps, as have been designed for the AMELIA vehicle are not recommended, and a more advanced design should be implemented. I believe that for a given flow and momentum coefficient, a flap can be designed with an angularly varying radius that reduces the amount of jet blowing power required to maintain flow attachment on the flaps and attain high lift.

Altogether, the work summarized in this report serves to highlight some of the problems that must be solved to design a truly optimized circulation control system.

# Appendix

## A) U duct Velocity Contours

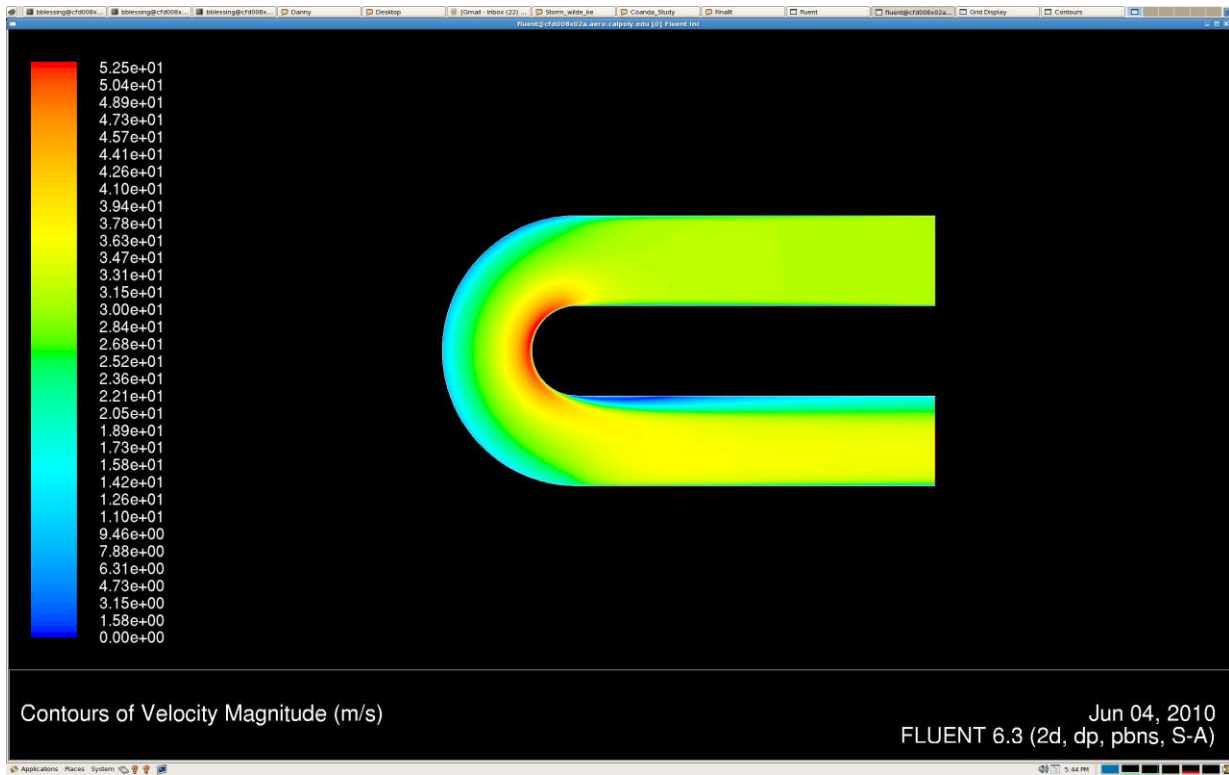


Figure 23. Spalart Allmaras

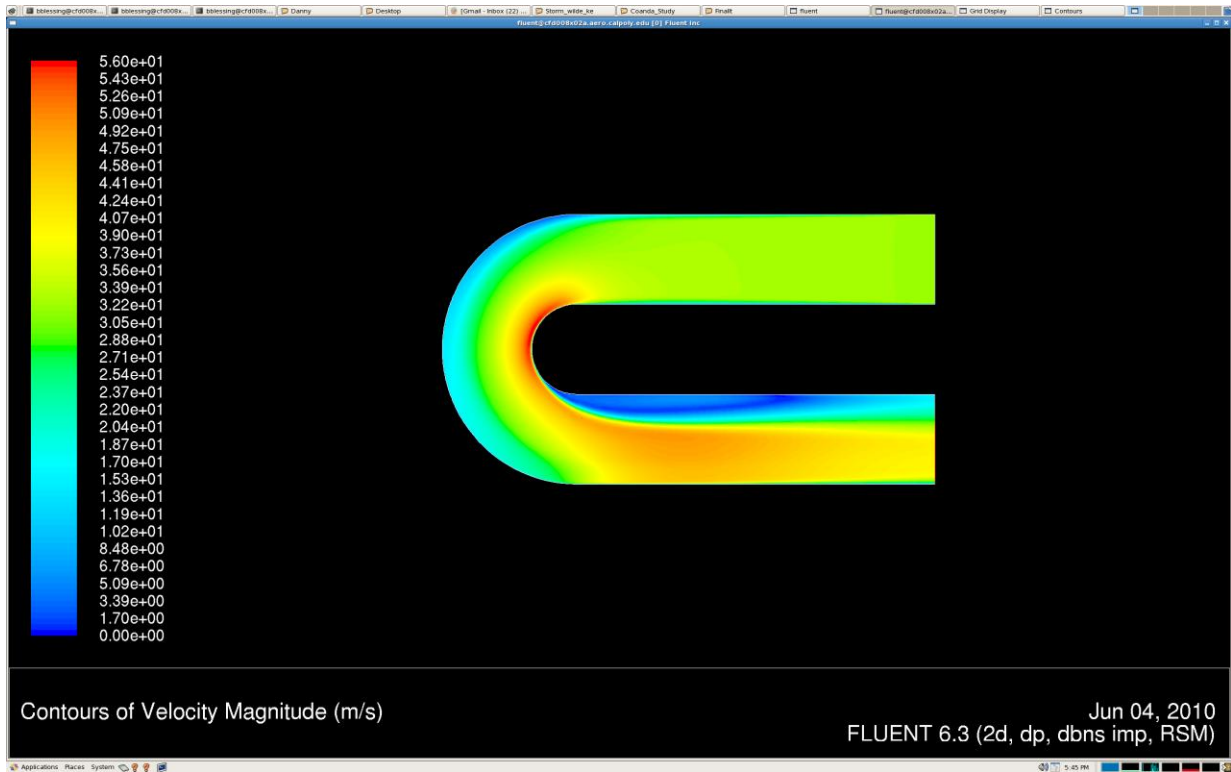


Figure 24. RSM

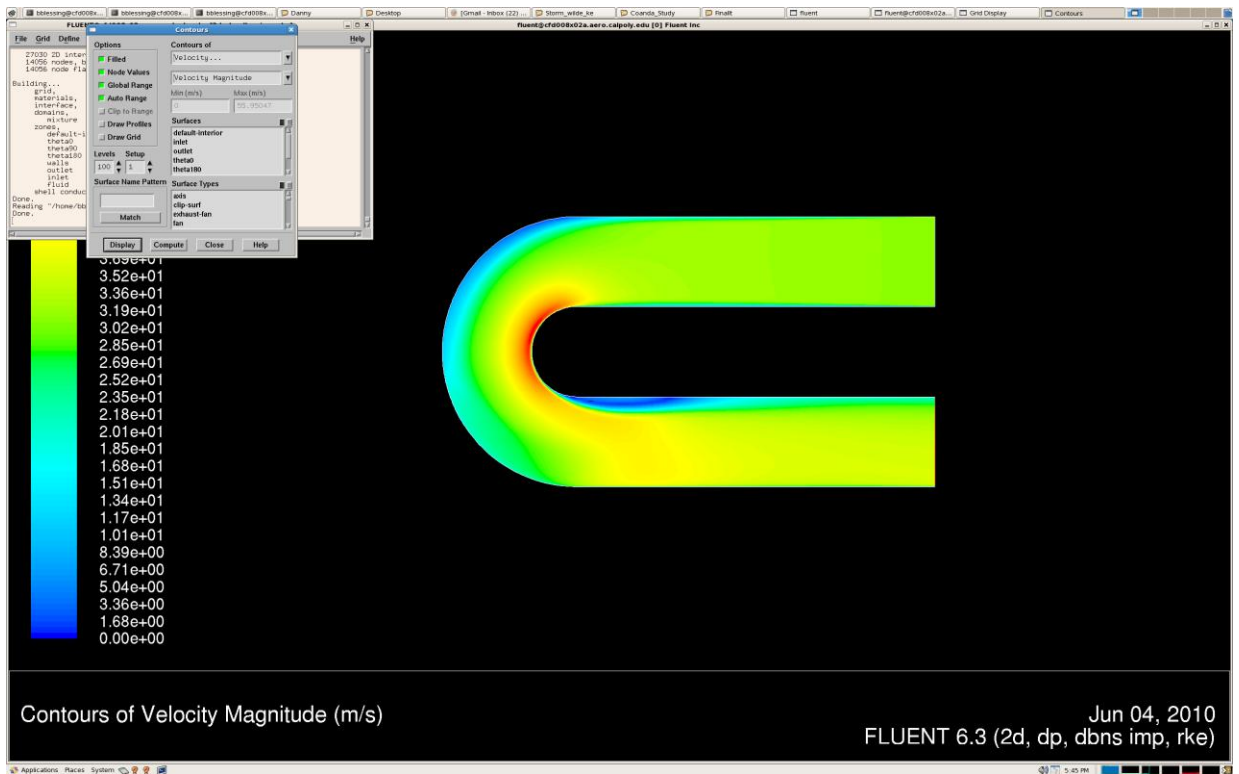


Figure 25. realizable k-ε

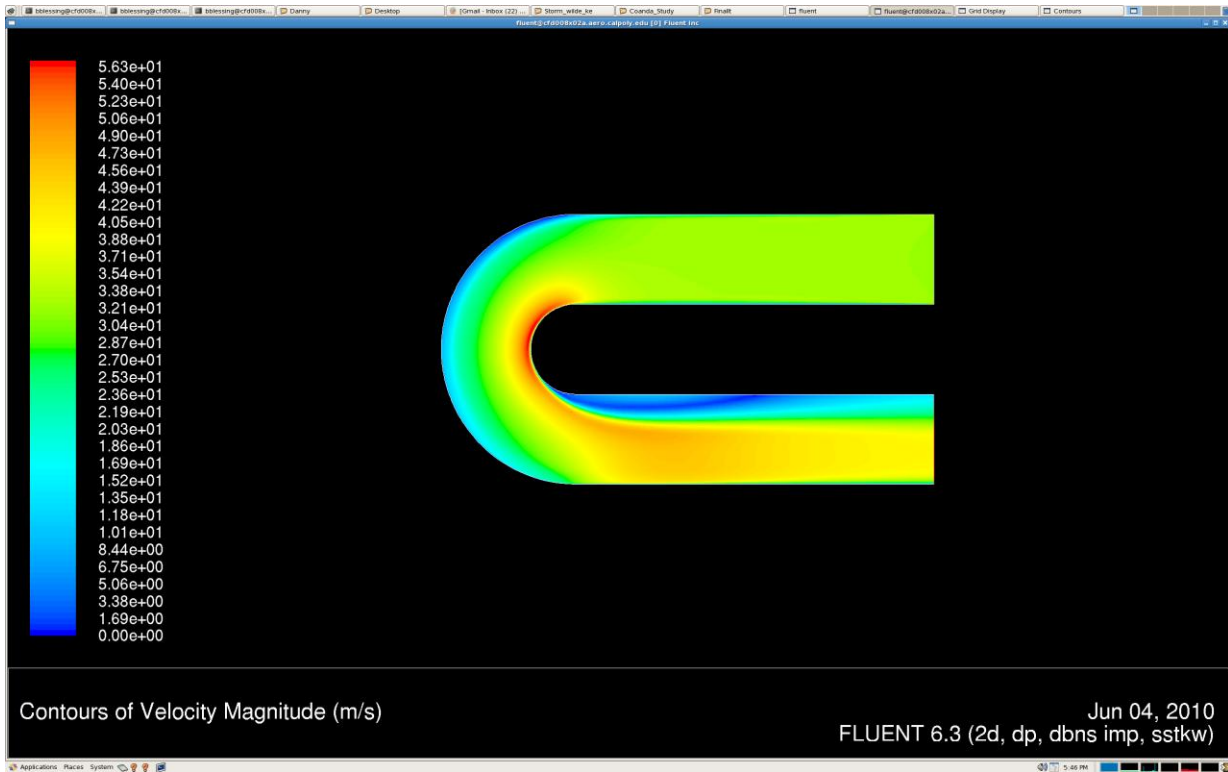


Figure 26.  $k-\omega$  SST



Figure 27. Standard  $k-\epsilon$

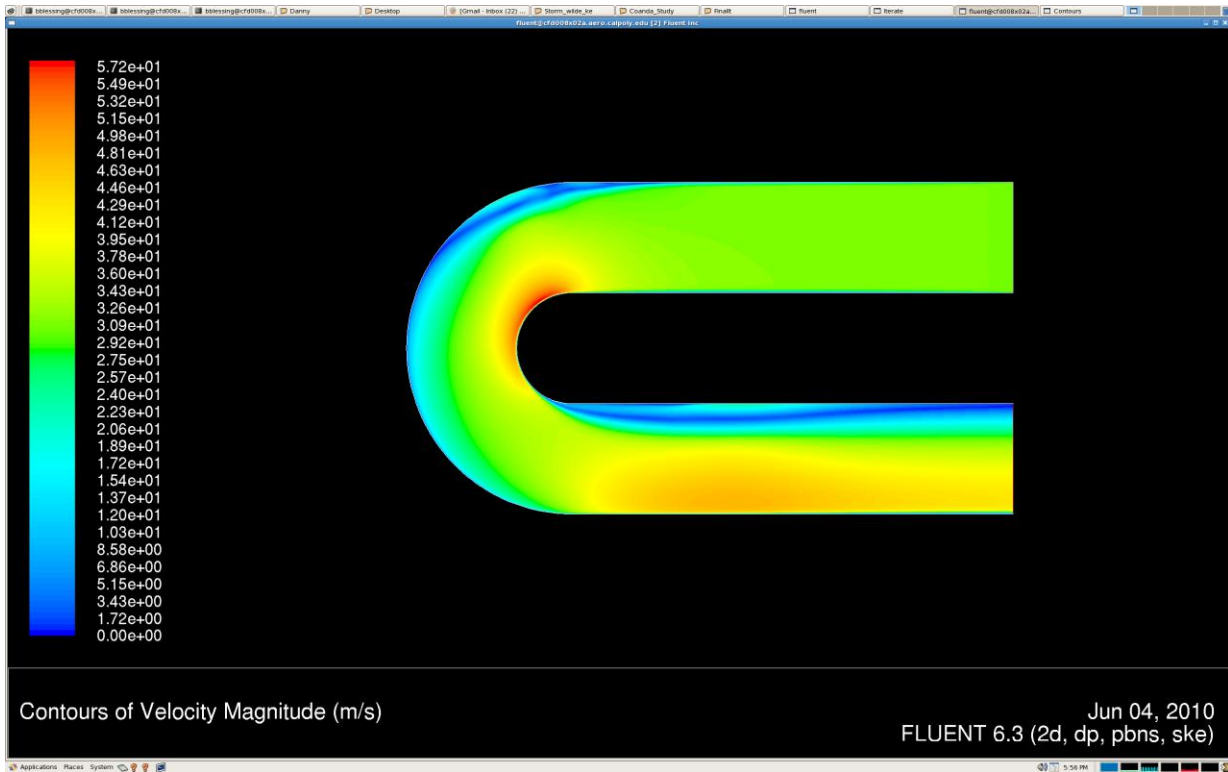


Figure 28.  $k-\epsilon v^2 f$  1<sup>st</sup> order linear

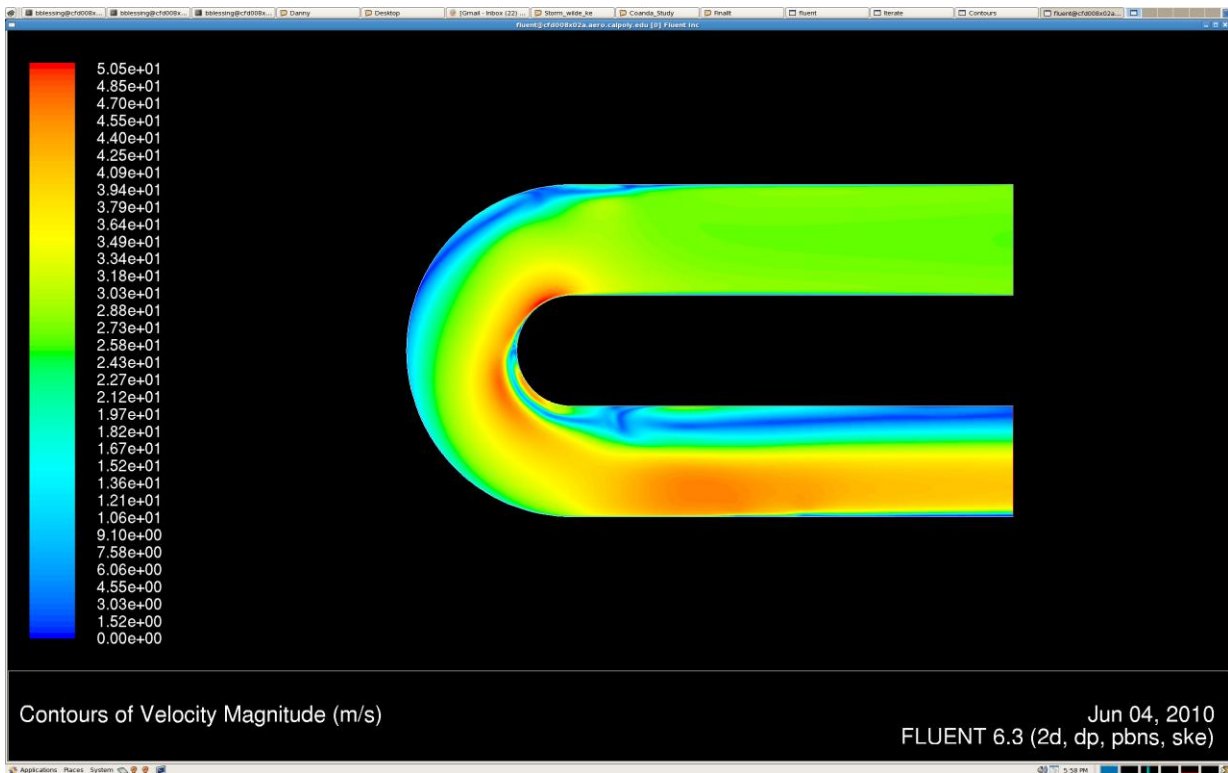


Figure 29.  $k-\epsilon v^2 f$  2<sup>nd</sup> order linear

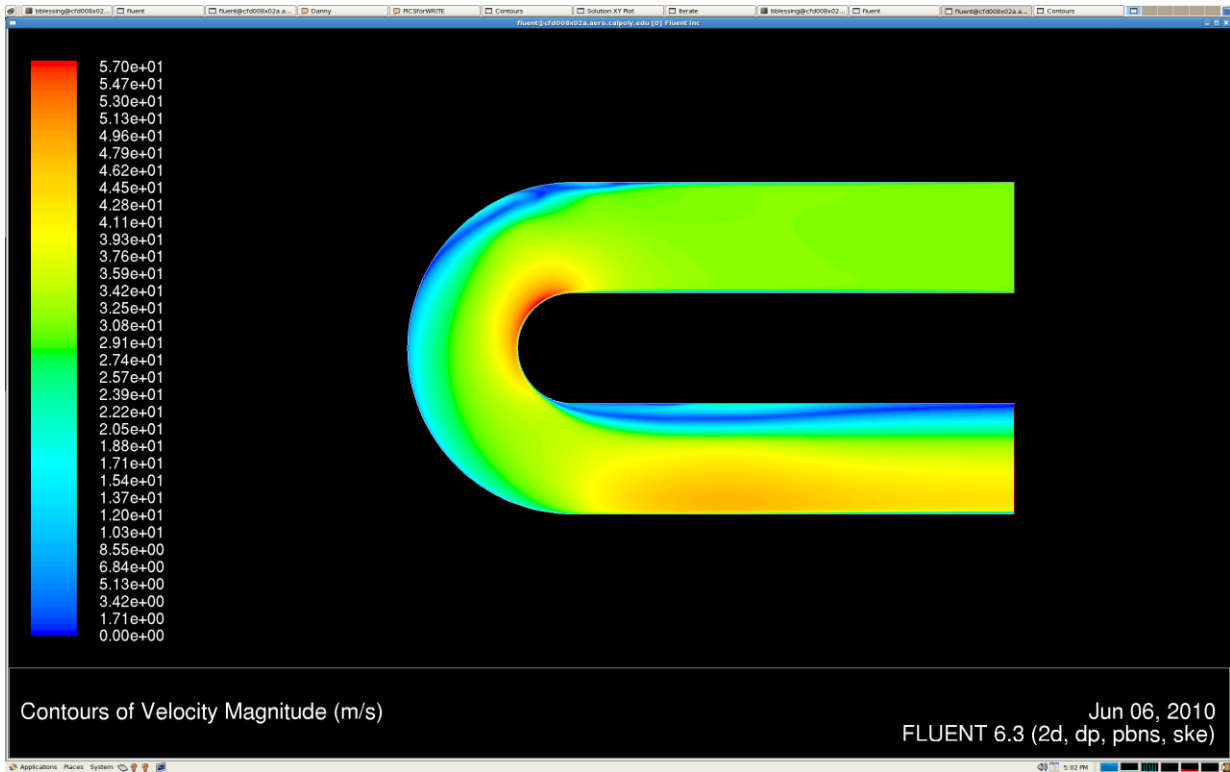


Figure 30.  $k-\epsilon v^2 f$  1<sup>st</sup> order nonlinear

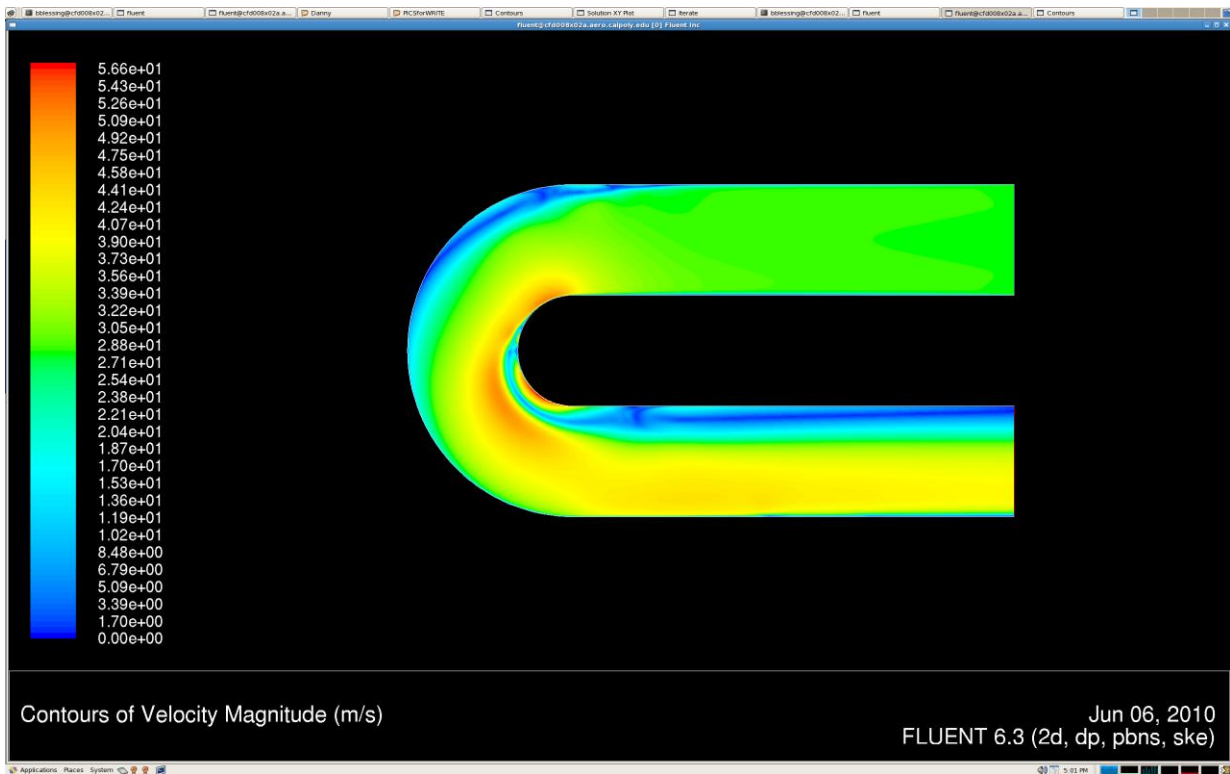
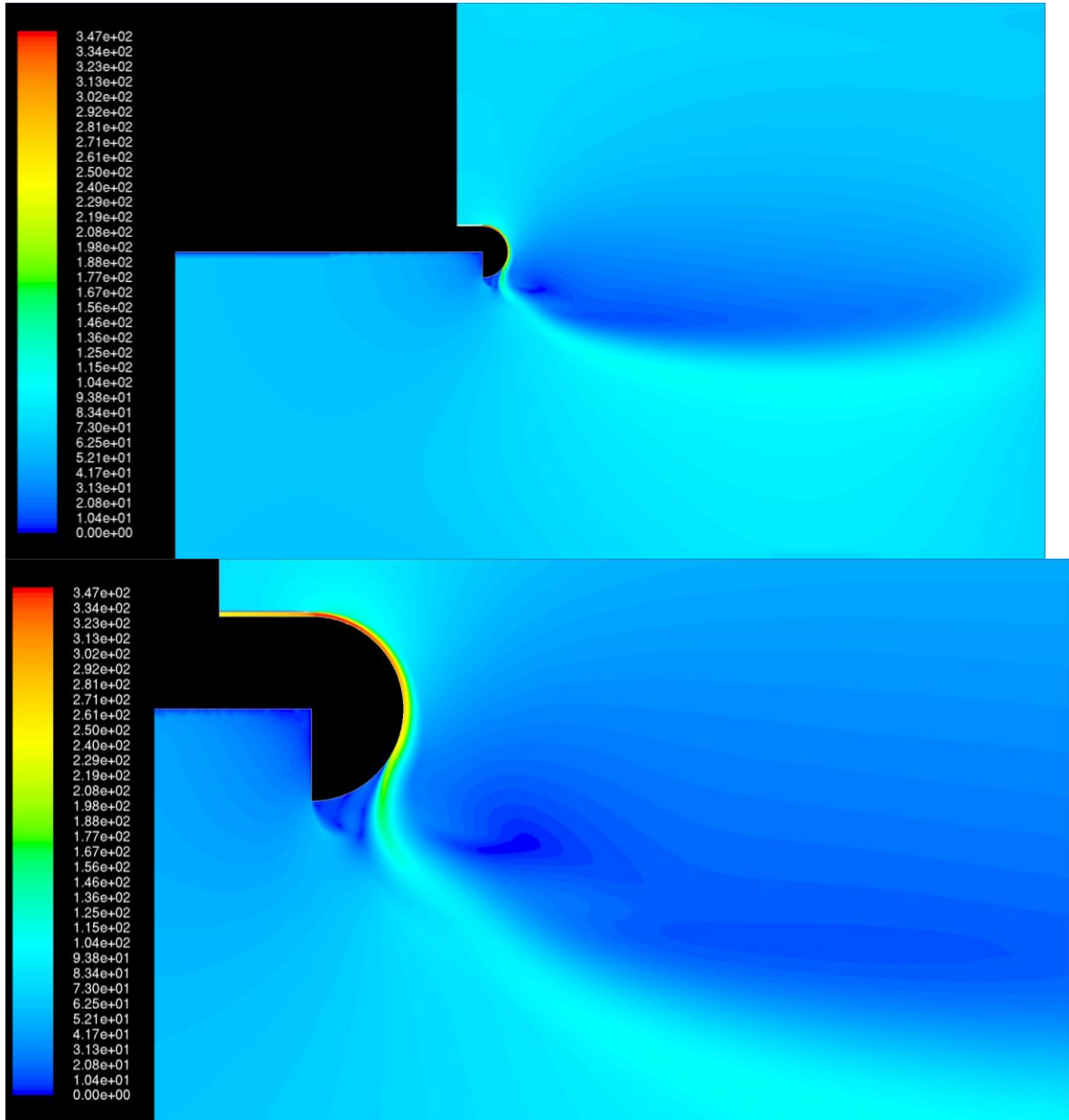


Figure 31.  $k-\epsilon v^2 f$  2<sup>nd</sup> order nonlinear

**B) Blown Flap Velocity Contours**



**Figure 32. Constant radius flap velocity contours**

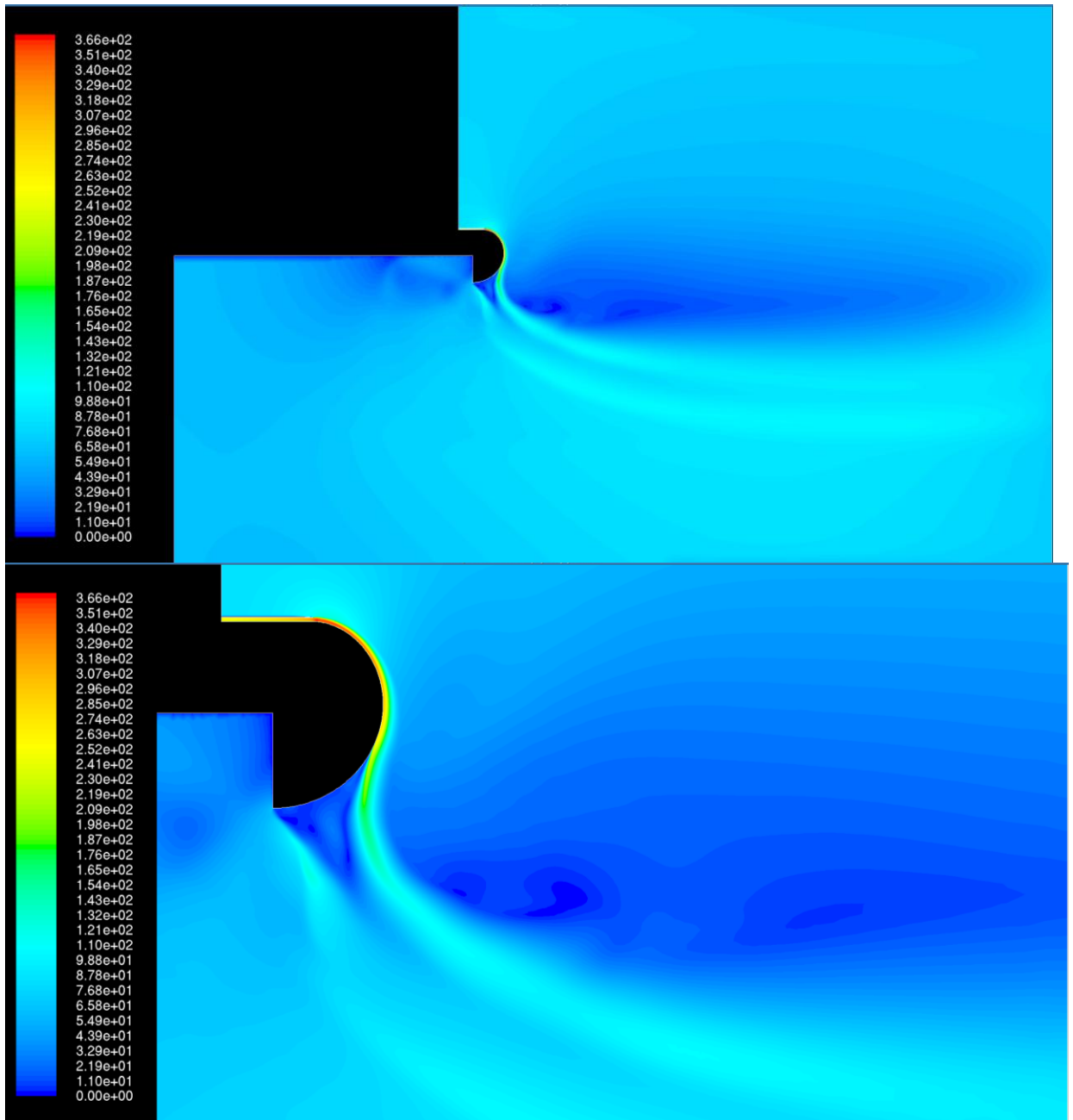


Figure 33. Dual radius 1 to 1.5 radius ratio flap velocity contours

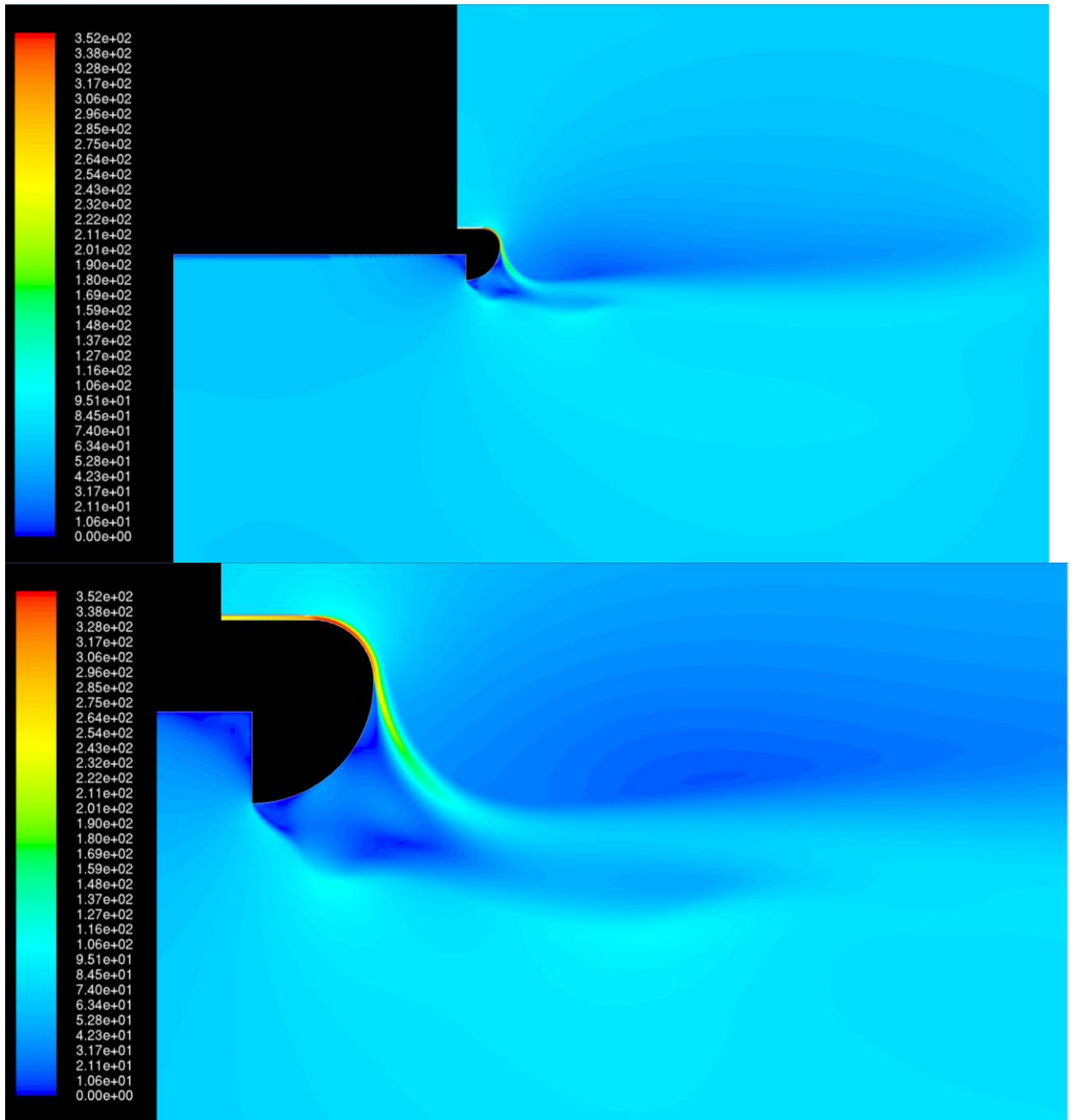


Figure 34. Dual radius 1 to 2 radius ratio flap velocity contours

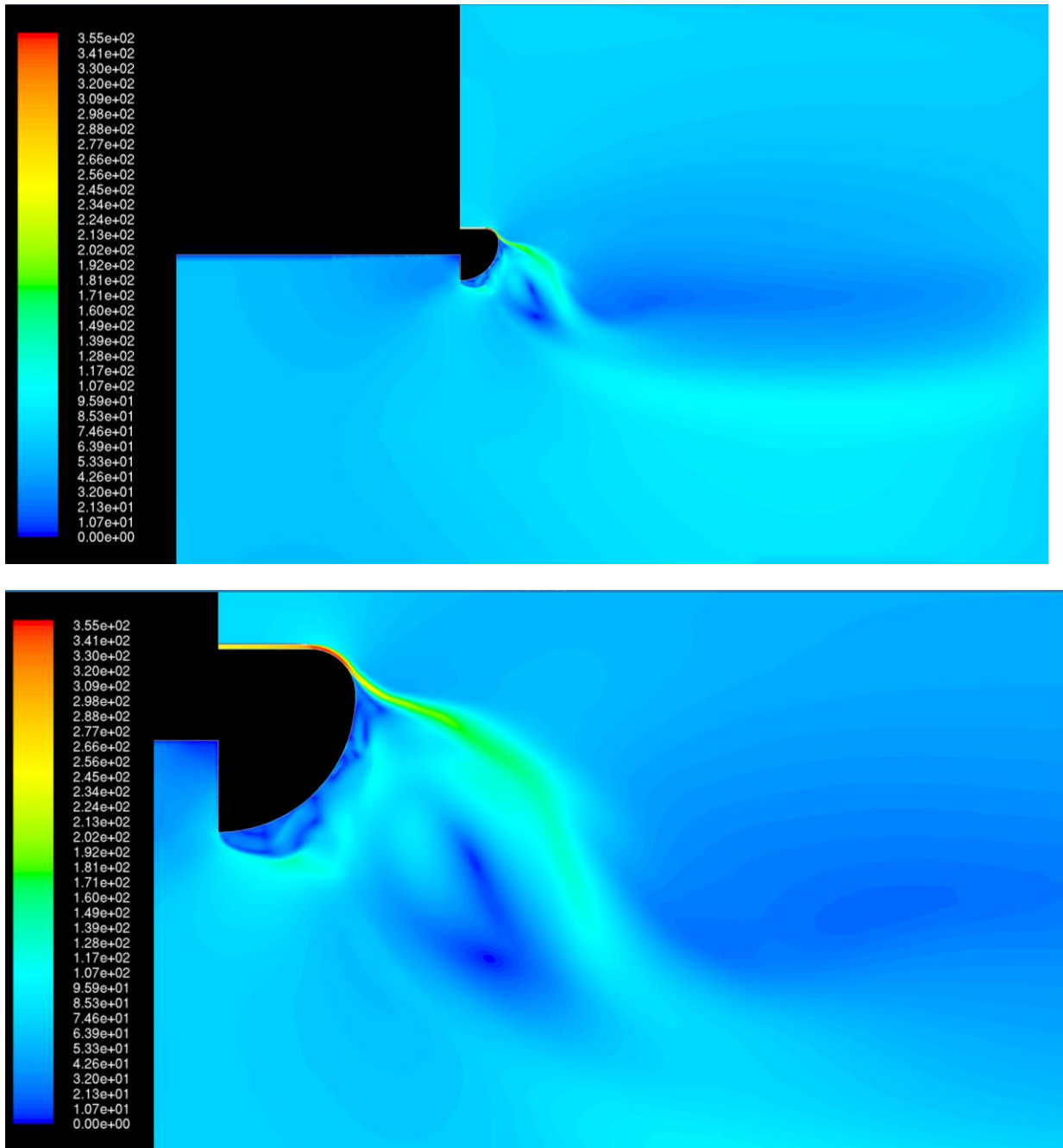


Figure 35. Dual radius 1 to 3 radius ratio flap velocity contours

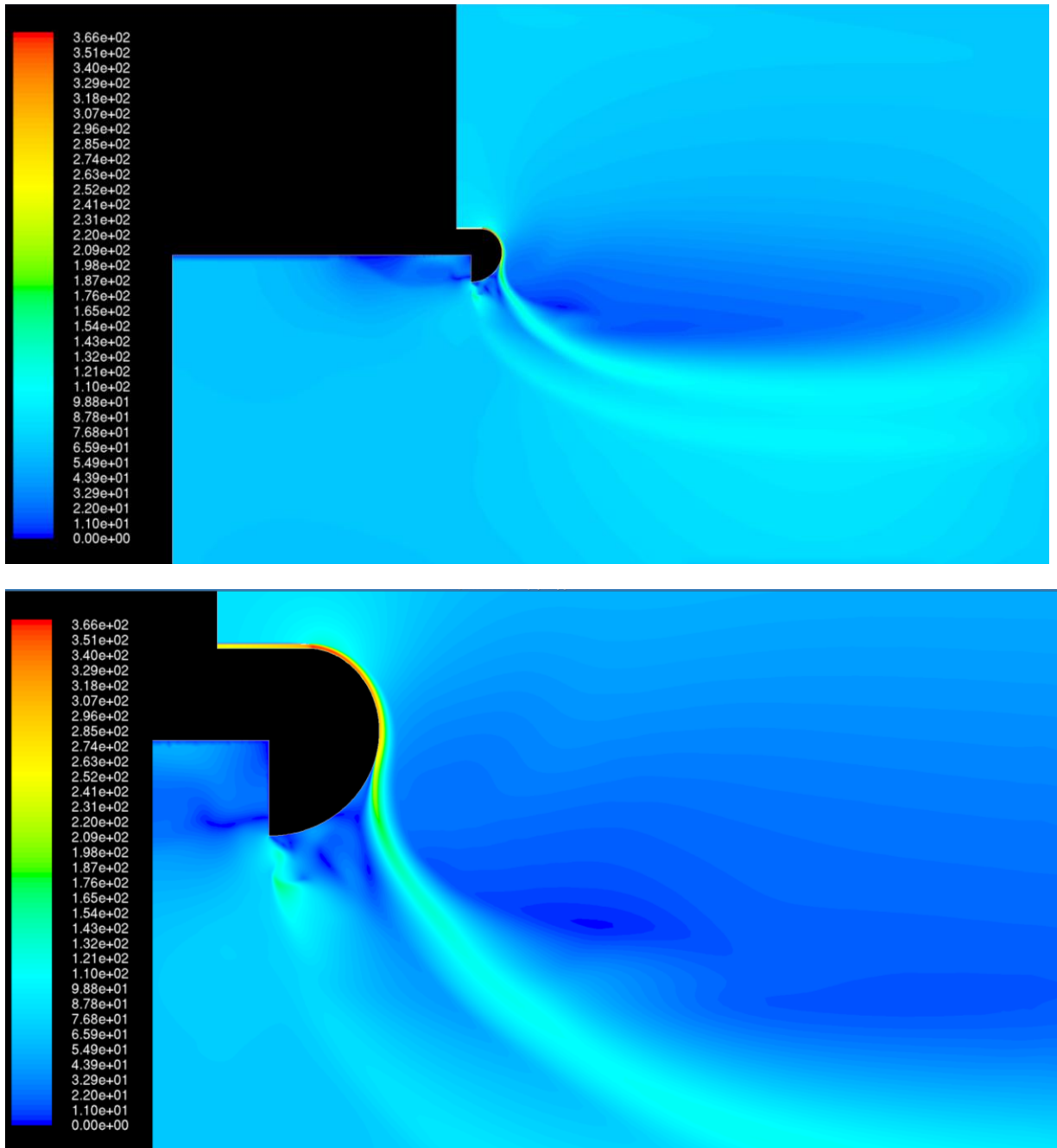


Figure 36. Linear 1 to 1.5 radius ratio flap velocity contours

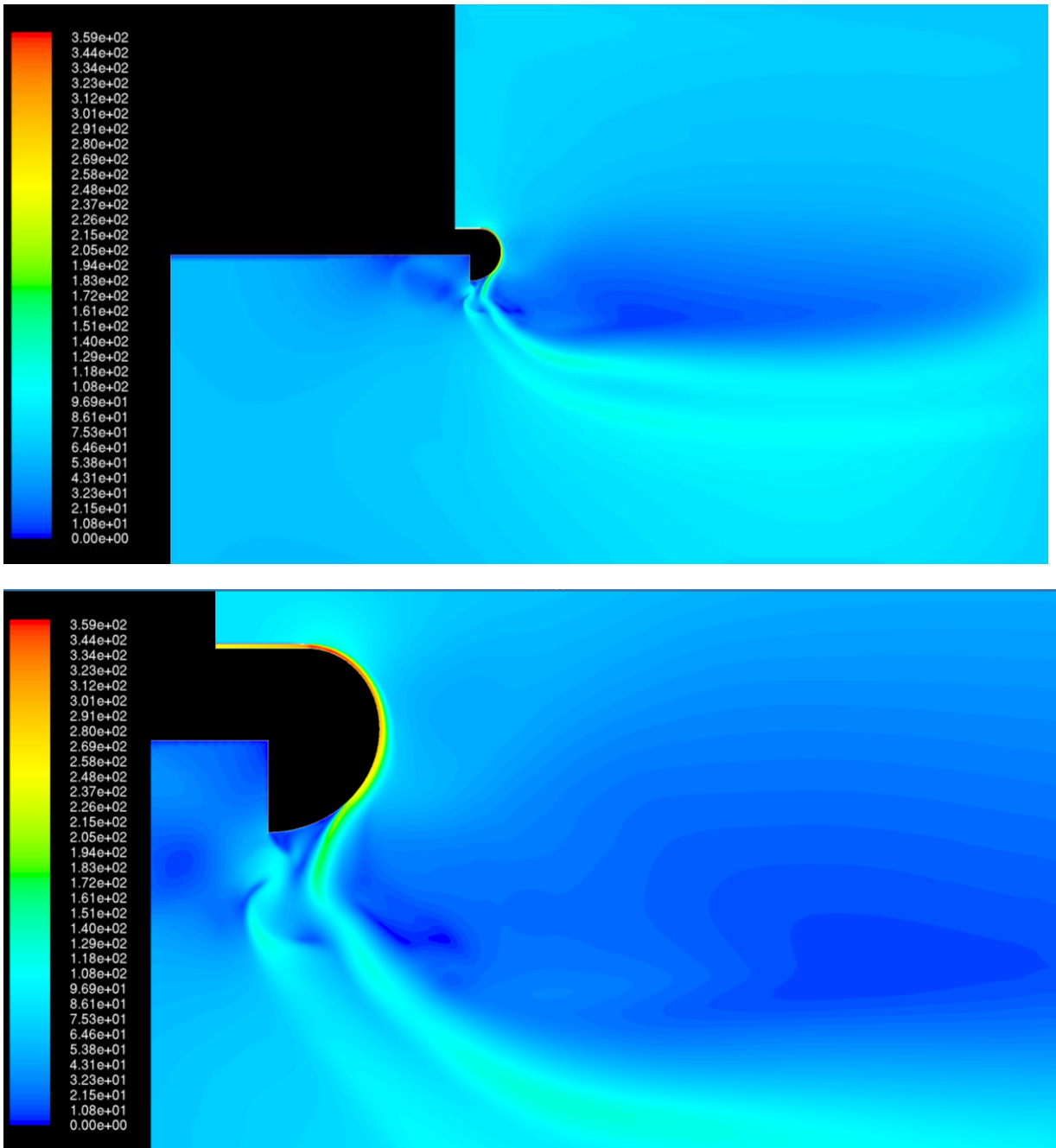


Figure 37. Linear 1 to 2 radius ratio flap velocity contours

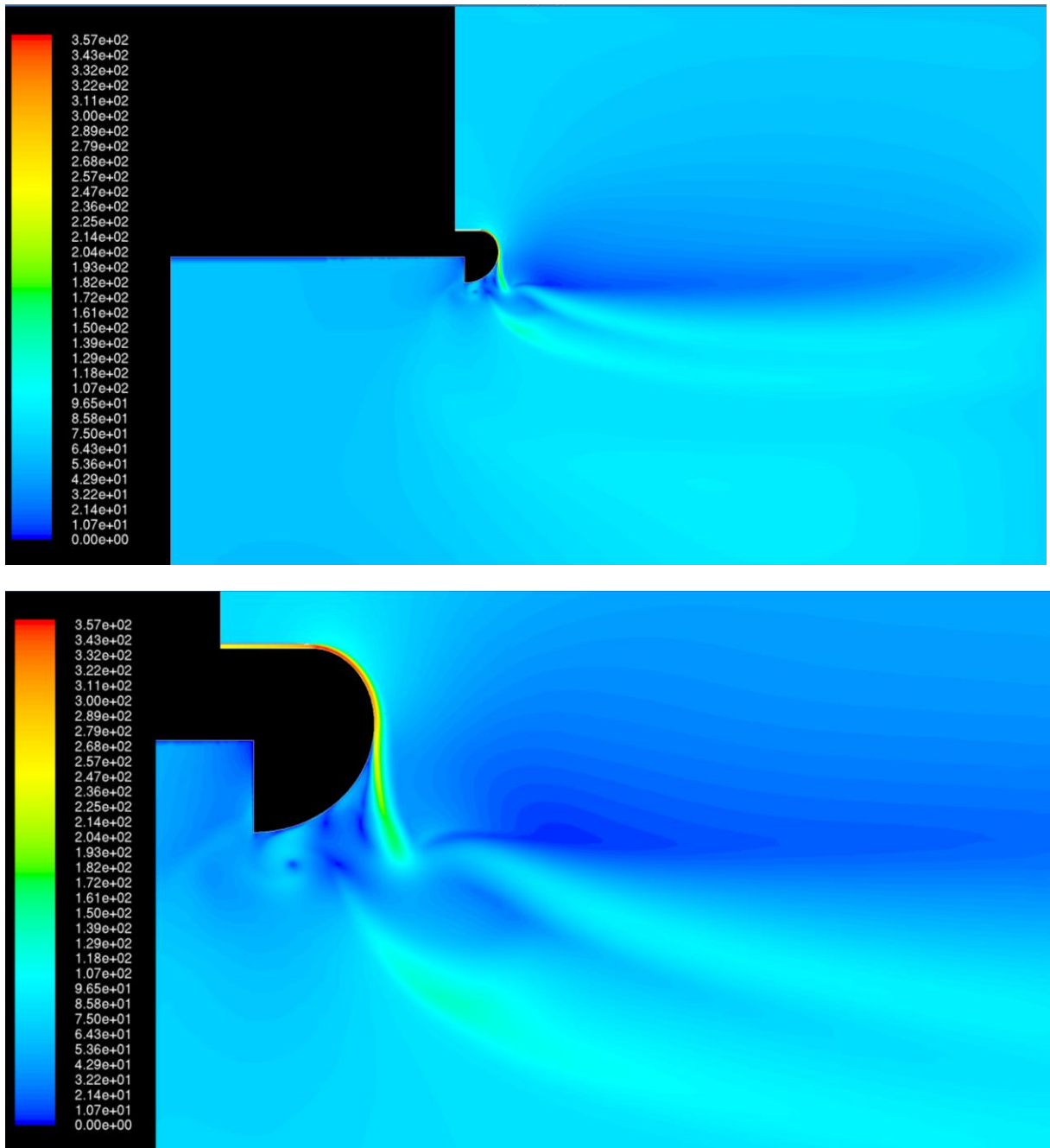


Figure 38. Linear 1 to 3 radius ratio flap velocity contours

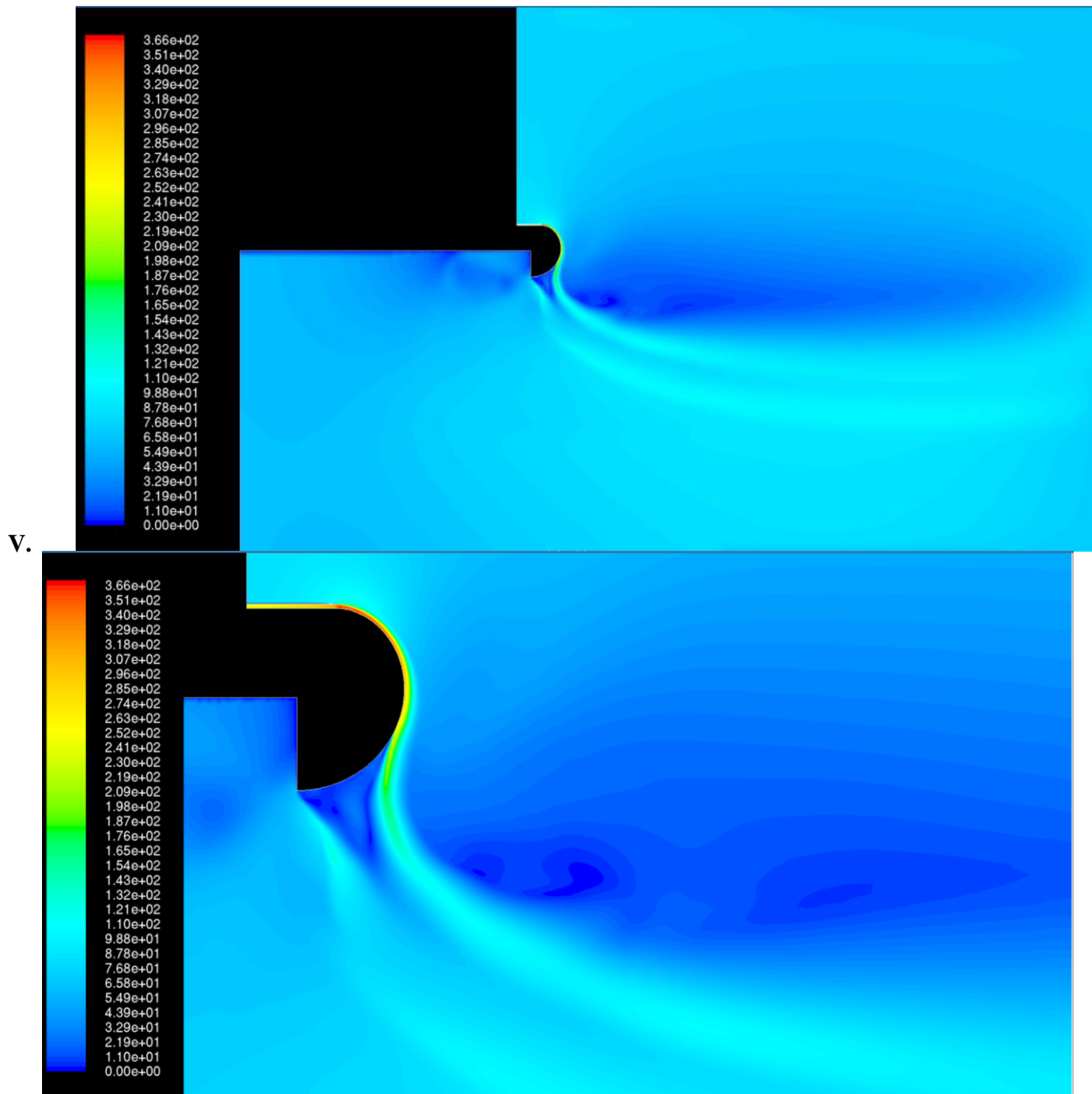


Figure 39. Quadratic 1 to 1.5 radius ratio flap velocity contours

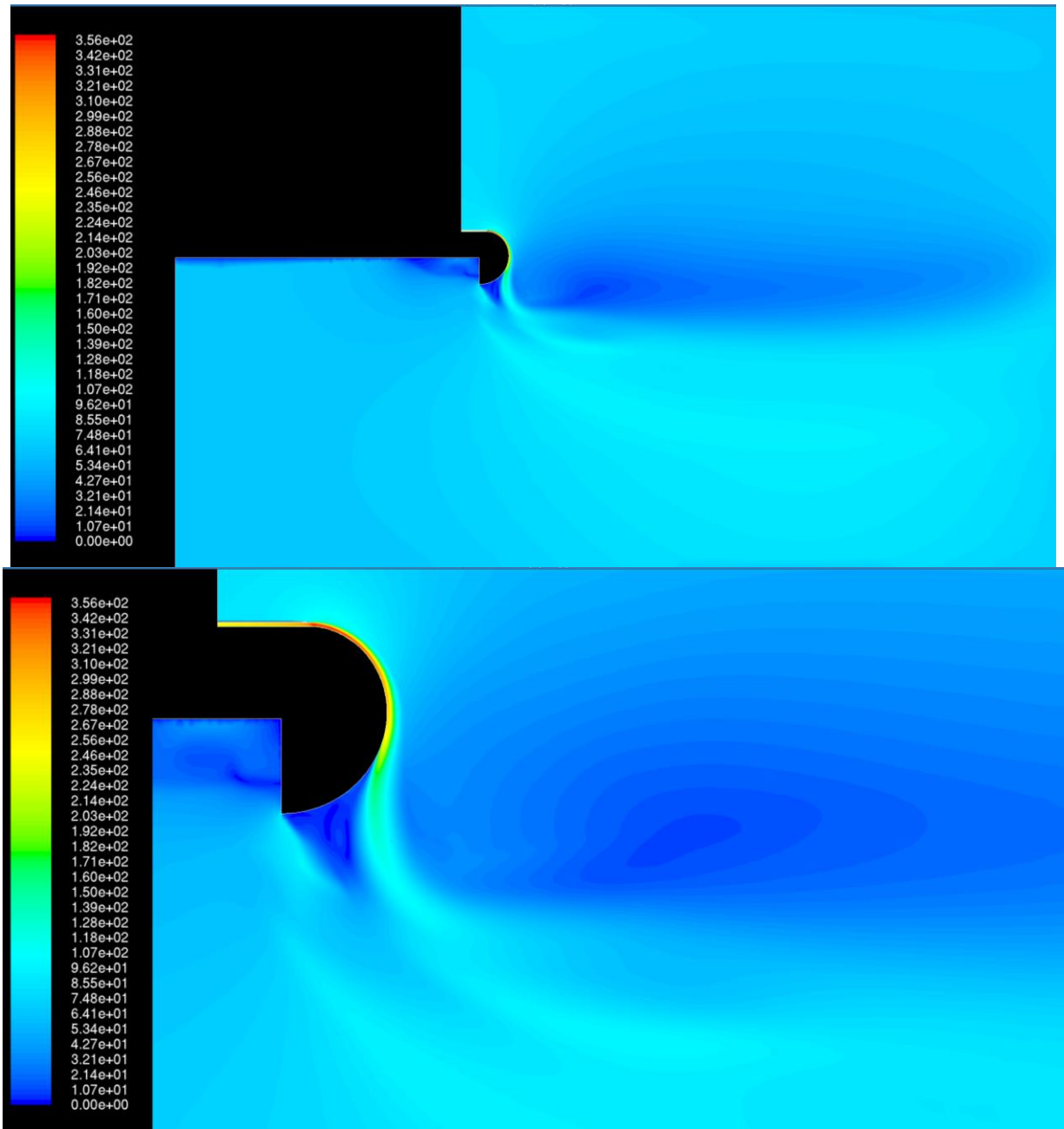


Figure 40. Quadratic 1 to 2 radius ratio flap velocity contours

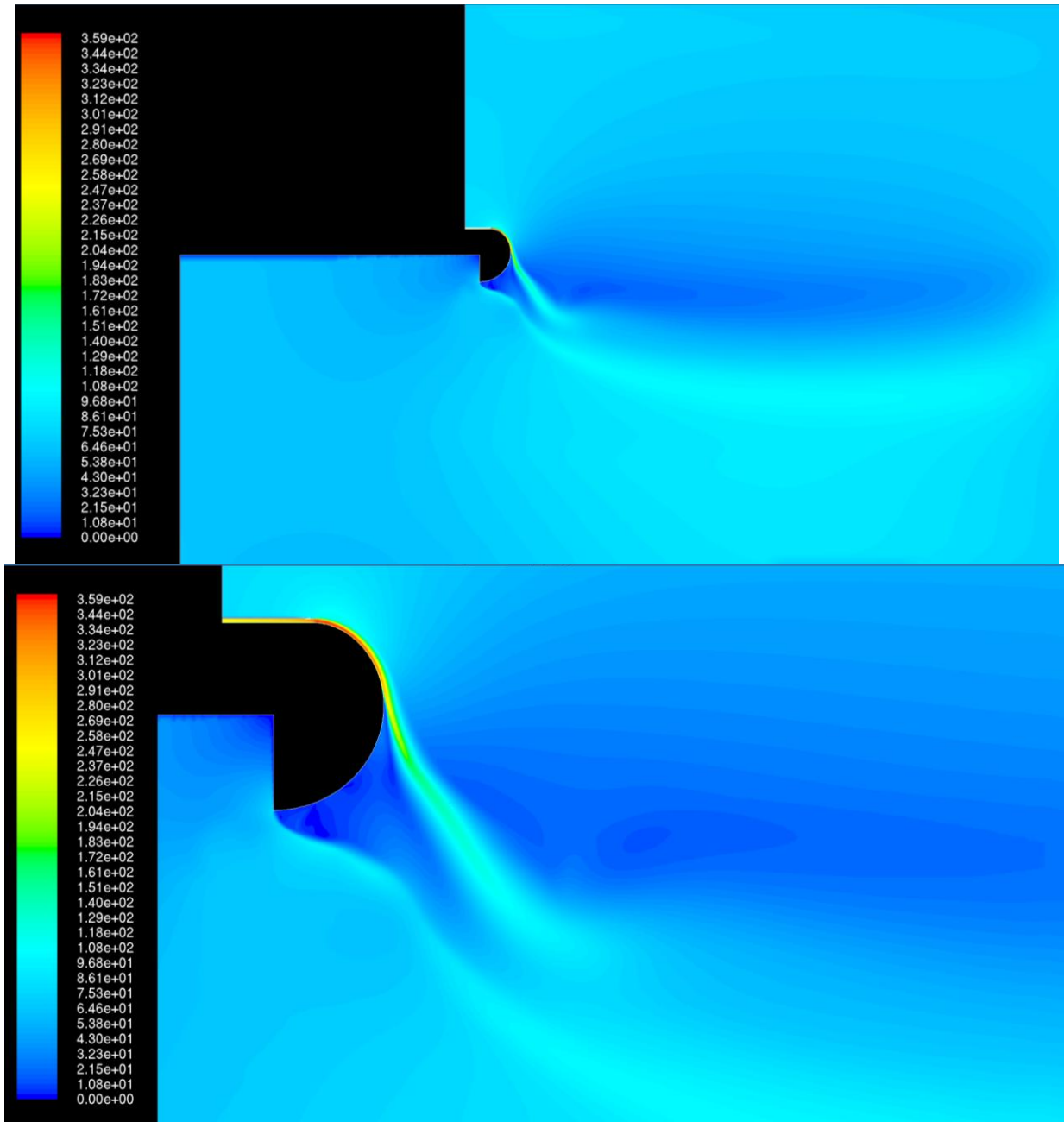


Figure 41. Quadratic 1 to 3 radius ratio flap velocity contours

## References

- [1] Rumsey, C.L, Gatski, T.B., “Isolating Curvature Effects in Computing Wall-Bounded Turbulent Flow,” AIAA Journal, 2001-0725
- [2] Monson, D.J., Seegmiller, “Comparison of Experiment with Calculation Using Curvature Corrected Zero and Two Equation Turbulence Models for a 2-dimensional U Duct,” AIAA Journal, 90-1484
- [3] Shur, M.L., Spalart, P.R., “Turbulence Modeling in Rotating and Curved Channels: Assessing the Spalart–Shur Correction” AIAA Journal Vol. 38 No. 5
- [4] Spalart, P.R. Shur, M. “On the Sensitization of Turbulence Models to Rotation and Curvature” Aerospace Science and Technology, 1997, no 5, 297-302
- [5] Moser, R.D., Moin, P. “Effects of curvature in wall-bounded turbulent flows” *Journal of Fluid Mechanics*, Vol. 175 (1987), pp. 479-510.
- [6] Bell, B., “Turbulent Flow Case Studies,” Fluent, Inc.
- [7] Bardina, J.E., Huang P.G., Coakley T.J. “Turbulence Modeling Validation” NASA Ames Research Center, Moffet Field, CA , 1997
- [8] Storm T.M., Marshall D.D., “Assessing the  $v^2$ -f Turbulence Models for Circulation Control Applications” California Polytechnic State University, San Luis Obispo, CA, 2010
- [9] Golden R.M., Marshall, D.D., “Design and Performance of Circulation Control Flap Systems” California Polytechnic State University, San Luis Obispo, CA, 2010
- [10] Marshall D.D., Jameson K.K., “Overview of Recent Circulation Control Modeling Activities at Cal Poly” California Polytechnic State University, San Luis Obispo, CA, 2010
- [11] Williams J.F., Cummings R.M., “Experimental Investigation of a Circular Cylinder under the Effects of Tangential Slot Blowing” California Polytechnic State University, San Luis Obispo, CA, 1996